

Suspended sediment properties in the Lower Mekong River, from fluvial to estuarine environments

Le, Hoang-Anh; Gratiot, Nicolas; Santini, William; Ribolzi, Olivier; Tran, Duc ; Meriaux, Xavier ; Deleersnijder, Eric; Soares-Frazão, Sandra

DOI

[10.1016/j.ecss.2019.106522](https://doi.org/10.1016/j.ecss.2019.106522)

Publication date

2020

Document Version

Accepted author manuscript

Published in

Estuarine, Coastal and Shelf Science

Citation (APA)

Le, H.-A., Gratiot, N., Santini, W., Ribolzi, O., Tran, D., Meriaux, X., Deleersnijder, E., & Soares-Frazão, S. (2020). Suspended sediment properties in the Lower Mekong River, from fluvial to estuarine environments. *Estuarine, Coastal and Shelf Science*, 233, 1-14. Article 106522. <https://doi.org/10.1016/j.ecss.2019.106522>

Important note

To cite this publication, please use the final published version (if applicable).
Please check the document version above.

Copyright

Other than for strictly personal use, it is not permitted to download, forward or distribute the text or part of it, without the consent of the author(s) and/or copyright holder(s), unless the work is under an open content license such as Creative Commons.

Takedown policy

Please contact us and provide details if you believe this document breaches copyrights.
We will remove access to the work immediately and investigate your claim.

1 Suspended sediment properties in the Lower Mekong River, from fluvial to 2 estuarine environments

3
4 **Hoang-Anh Le** ^{1,2}, **Nicolas Gratiot** ^{2,3,*}, **William Santini** ⁴, **Olivier Ribolzi** ⁴, **Duc Tran** ⁵,
5 **Xavier Meriaux** ⁶, and **Eric Deleersnijder** ^{7,8}, **Sandra Soares-Frazão** ¹

6
7 ¹ Civil and Environmental Engineering, Institute of Mechanics, Materials and Civil Engineering (IMMC),
8 Université catholique de Louvain, Place du Levant 1, B-1348 Louvain – la – Neuve, Belgium

9 ² Asian Research Center on Water (CARE-Rescif), Ho Chi Minh City University of Technology, Block B7, 268
10 Ly Thuong Kiet Street, District 10, Ho Chi Minh City, Vietnam

11 ³ CNRS, IRD, IGE, Université Grenoble Alpes, F-38000 Grenoble, France

12 ⁴ Géosciences Environnement Toulouse (GET), Université de Toulouse, IRD, CNRS, UPS, Toulouse, France

13 ⁵ Faculty of Environment and Natural Resources, Ho Chi Minh City University of Technology, VNU-HCM,
14 268 Ly Thuong Kiet, Ho Chi Minh City, Vietnam

15 ⁶ Université Littoral Côte d'Opale, Université Lille, CNRS, UMR 8187, LOG, Laboratoire d'Océanologie et de
16 Géosciences, F 62930Wimereux, France

17 ⁷ Université catholique de Louvain, Institute of Mechanics, Materials and Civil Engineering (IMMC) & Earth
18 and Life Institute (ELI), 4 avenue Georges Lemaître, B-1348 Louvain-la-Neuve, Belgium

19 ⁸ Delft University of Technology, Delft Institute of Applied Mathematics (DIAM), Van Mourik Broekmanweg
20 6, 2628XE Delft, The Netherlands

21
22 * Correspondence: nicolas.gratiot@ird.fr; Tel.: +84-9-4129-4232

23
24 **Abstract:** The Mekong river is one of the largest rivers in the world, which flows through
25 six countries of Southeast Asia (China, Myanmar, Laos, Thailand, Cambodia and Vietnam).
26 Its hydro-sedimentary regime is changing rapidly, as a consequence of a regional shift of
27 land use (agriculture, road, etc.), damming, sand mining and climate changes, among others.
28 This study assesses the behavior of particles transported in suspension in the Lower Mekong
29 River (LMR), along approximately 1700 km from fluvial to estuarine environments.
30 Suspended sediment properties were estimated, simultaneously with hydrodynamic
31 conditions, during three field campaigns. In addition, further investigations were performed
32 in the laboratory to assess the structures of particles (flocculated or not), their capacity to
33 flocculate (and the impacts on siltation), under a wide range of sediment concentration (400
34 to 4000 mg.L⁻¹). This study confirms that suspended sediment transported in the LMR are
35 predominantly (75 % by volume) flocculi (or freshly eroded soils aggregates), with median

60
61
62 36 aggregated particle size in the range 10 - 20 μm and median settling velocity of the order of
63
64 37 0.01 – 0.1 $\text{mm}\cdot\text{s}^{-1}$. These flocculi are robust under the hydrodynamic conditions (turbulence
65
66 38 and suspended sediment concentration – SSC) existing in the LMR. Laboratory
67
68 39 investigations reveal the existence of a threshold sediment concentration (400 $\text{mg}\cdot\text{L}^{-1}$),
69
70 40 beyond which flocculation and sedimentation increase of orders of magnitudes. Thus,
71
72 41 concentration that exceeds this threshold might promote the formation of so-called fluid mud
73
74 42 layers. Because of the nonlinear response of flocculation and sedimentation with SSC and
75
76 43 considering the ongoing changes at a regional scale in the LMR, higher occurrence of fluid
77
78 44 mud layers in the fluvial upstream waterbodies might be anticipated, and a lower occurrence
79
80 45 in estuaries and alongshore where the concentration decrease. The geomorphology could be
81
82 46 impacted, with an over-siltation in dams and an exacerbated erosion of the muddy-mangrove
83
84 47 coast.

85
86
87 48 **Keywords:** Mekong; LISST; SCAF; fluid mud layer; flocculation, settling velocity
88
89 49

90 50 **1. Introduction**

91 51 The Mekong river is the tenth longest river in the world with a length of 4909 km and has a
92 52 basin area of 795,000 km^2 . Its mean annual discharge is approximately 475 km^3 , i.e. the sixth
93 53 largest in the world. The river originates from the Tibetan Plateau (China) with an elevation of
94 54 more than 5000 m above sea level (a.s.l.); then, the river flows through a variety of
95 55 geomorphological and climatic systems and ends in the fertile delta of Vietnam (55,000 km^2),
96 56 before discharging into the South East Sea of Vietnam (Mekong River Commission portal -
97 57 MRC, www.mrcmekong.org/). Under human pressures and climate change, the river is facing
98 58 many serious issues in link with changes in sediment dynamics. One of the most evident
99 59 transformation is the construction of large hydropower dams in the upstream Mekong, which
100 60 are modifying the hydrological cycle, and reducing the sediment discharge into the floodplain
101 61 and estuaries at an alarming point (Schmitt et al., 2017). Sand mining in the delta is also a
102 62 direct threat for the hydro-sedimentary budget. According to the literature, sediment flux has
103 63 already decreased by almost five fold over 35 years, from about 160 mill. $\text{tons}\cdot\text{year}^{-1}$ in 1983
104 64 (Milliman et al., 1983) to 87.4 ± 28.7 mill. $\text{tons}\cdot\text{year}^{-1}$ in 2005 (Darby et al., 2016 and Schmitt
105 65 et al., 2017) and 40 ± 20 mill. $\text{tons}\cdot\text{year}^{-1}$ in 2015 - 2016 (Thi Ha et al., 2018).
106
107
108
109
110
111
112
113
114
115
116
117
118

119
120
121
122
123
124
125
126
127
128
129
130
131
132
133
134
135
136
137
138
139
140
141
142
143
144
145
146
147
148
149
150
151
152
153
154
155
156
157
158
159
160
161
162
163
164
165
166
167
168
169
170
171
172
173
174
175
176
177

66 Sand mining, trapping by dams, and the resulting reduction of sediment flux are undoubtedly
67 corroborated with some changes in the nature (and populations) of particles transported. Some
68 expected consequences in geomorphology, floodplain fertility and pollutant dynamics are
69 already evoked (Kondolf et al., 2018), but need to be better studied. Previous studies
70 conducted in the LMR indicated that the upper fluvial section was dominated by two particles
71 size populations: silts, with a diameter of 10 - 20 μm ; and sands, with a diameter of 63 - 200
72 μm , accounting for 78 % and 22 % of the total particle load, respectively (Peteuil et al., 2014).
73 Downstream, in the estuary, flocculated fine particles dominate. The observed floc size,
74 reported in the literature, was 30 - 40 μm , constituting 60 - 80 % of the total sediment load in
75 high flow season. However, in the low flow season, the floc size increased to 50 - 200 μm ,
76 accounting for 70 - 80 % of the total volume (Wolanski et al., 1996 and Wolanski et al.,
77 1998). This observed variability of sediment properties reflects a direct adjustment of physical
78 properties along streams, which operates at microscopic scales (flocculation, sedimentation
79 and erosion), in link with hydrodynamic conditions and their seasonal variations. The
80 different origins, together with different physicochemical and biological conditions between
81 the sites, cause difficulties in interpreting the results.

82 Particle size, settling velocity and their spatio-temporal evolution through flocculation, are
83 fundamental properties that need to be estimated to assess sediment transport and deposition
84 processes in space and time (Manning et al., 2011a; Winterwerp, 2002). This is particularly
85 true in the case of mud/sand mixtures, where complex interactions occur and need to be
86 characterized for a realistic understanding of sediment dynamics (Manning et al., 2010).
87 Conceptually, flocculation develops from primary particles into hierarchical structures,
88 namely flocculi, microflocs and macroflocs. Primary particles mainly consist of fine particles
89 with sizes of 1 - 6 μm , and can be organic or inorganic. They aggregate to form 1st order
90 structures, so-called flocculi, with diameters of the order of 6 - 50 μm . They are usually
91 hardly broken down into primary particles, even at the highest turbulent shear modulus
92 experienced by particles in large rivers. Thus, it is generally considered that flocculi are a
93 major component of sediment dynamics. Microflocs form the 2nd order of aggregation. They
94 include primary particles and flocculi and have sizes of 50 - 200 μm . Finally, macroflocs are
95 the largest particle structures. They are loose structures with a wide size distribution, ranging
96 from hundreds to thousands of micrometers (Lee et al., 2012 and Fettweis et al., 2006). Flocs
97 (micro and macro) are generally fragile structures, easily broken down when passing through
98 high turbulent shear modulus (Manning et al., 2011a).

178
179
180
181
182
183
184
185
186
187
188
189
190
191
192
193
194
195
196
197
198
199
200
201
202
203
204
205
206
207
208
209
210
211
212
213
214
215
216
217
218
219
220
221
222
223
224
225
226
227
228
229
230
231
232
233
234
235
236

99 Flocculation at microscopic scale, as some hydro-sedimentary and geomorphological impacts
100 at scales of river reaches, estuaries and deltas, in particular because it promotes the formation
101 of fluid mud layers. Fluid mud is defined as a mixture of high-concentrated fine sediments
102 with water (Bachmann et al., 2005). It is generated by liquefaction of cohesive sediment beds
103 by waves or by an imbalance between settling and eddy diffusion near the bed, or by the
104 convergence of sediment fluxes from upstream and downstream. In energetic environments,
105 large particles such as sand are also found in fluid mud samples, but the portion is less than
106 few percent (McAnally et al., 2007). Fluid mud masses may be advected over large distances
107 horizontally without losing their coherent nature or internal chemical properties; and its
108 horizontal convergence may often be a key mechanism of their accumulation (McAnally et
109 al., 2007). Thus, fluid mud in thin layers is considered as an intermediate stage of deposition
110 (before formation of consolidated bed layers) or bed erosion (under entrainment process by
111 fluidization (McAnally et al., 2007). Its thickness varies from few centimeters to meters
112 (Sottolichio et al., 2011; Azhikodan et al., 2018).

113 The occurrence of fluid mud is commonly observed in quiescent environments such as lakes
114 and reservoirs (Mehta et al., 1991; McAnally et al., 2007) or in the Estuarine Turbidity
115 Maximum zones (ETM) (Uncle et al., 2006; Winterwerp et al., 2011; Azhikodan et al., 2018)
116 such as estuaries, navigation channels, harbour basins or along muddy coasts all over the
117 world (Bachmann et al., 2005; Schelske et al., 2006; Gratiot et al. 2007; Toorman et al. 2018).
118 The turbidity maximum zone is often created by resuspension from the bed during parts of the
119 tidal cycle and shows a significant drag reduction at high SSC concentration gradient (Dyer et
120 al., 2002a and Dyer et al., 2002b). However it has been poorly studied and reported in the
121 literature dedicated to the LMR (Wolanski et al., 1998, Xue et al., 2010) and received some
122 more interest recently (Gugliotta et al., 2019; Nittrouer et al., 2017; Gratiot et al., 2017).

123 This study originally combines in situ measurements and laboratory investigations to examine
124 the physics of particles (especially flocculation properties, measured with new patented
125 equipment developed by SCAF®) and to understand transport/deposition processes in the
126 LMR. Sampling and analyses are performed in three contrasted environments: an upper
127 fluvial reach in Laos (Fig. 1b), a lacustrine environment in Cambodia (Fig. 1c) and an
128 estuarine environment in Vietnam (Fig. 1d). The same methodology was applied for these
129 three contrasted environments (upstream river, lake and estuary). Results obtained allow for
130 answering and discussing the following points:

- 237
238
239 131 • Are suspended sediment flocculated or not (percentages of cohesive versus non-
240 132 cohesive particles transported in suspension)?
241
242
243 133 • If yes, are floc populations stable from upstream to downstream and/or highly
244 134 dependent on hydrodynamic conditions (SSC, turbulence, salinity)?
245
246
247
248 135 • Are suspended sediment predominantly transported as washload (single path with no
249 136 bed interactions), or does it experience successive phases of deposition and erosion?
250
251
252 137 • How much SSC increase can modify flocculation, sedimentation and how much this
253 138 could contribute to the formation of fluid mud layers and, finally, modify the
254 139 geomorphology of the LMR?

255
256
257 140 By answering to the four questions above, the paper proposes a better understanding of the
258 141 physical properties of sediment and their transportation modes along the Lower Mekong
259 142 River. Because flocculation and fluid mud layers are playing an important role in the dynamic
260 143 of the Mekong Delta, this information will facilitate the implementation of integrated tools,
261 144 such as ecological/geomorphological models, to go through a better management of large
262 145 scale hydrosystems.

266 146 **2. Study areas and Methods**

267 147 *2.1. Study area*

268
269
270 148 Field investigations have been conducted at three locations of the LMR, assumed to be
271 149 representative of river morphological units, from the upper fluvial environment to the
272 150 lacustrine and the estuarine environments (Fig. 1a).

273 151 *2.1.1. Fluvial environment*

274 152 The upper fluvial reach considered is located at the level of Luang Prabang city, Laos
275 153 (Fig.1b). It is situated on a long stem at the confluence of the Mekong and Nam Khan rivers, a
276 154 tributary of the Mekong. Its altitude is approximately 300 m a.s.l. This area is covered with
277 155 steep hillsides and has been experiencing drastic land use changes, predominantly leading to
278 156 erosion, since the last decades (Ribolzi et al., 2017). At Luang Prabang, the Mekong river
279 157 section is already wide, with width of 600 - 700 m. However, when passing through gorges,
280 158 the channel becomes swiftly narrow, approximately 100 m wide, and bounded by limestone

281
282
283
284
285
286
287
288
289
290
291
292
293
294
295

296
297
298 159 pavement. The channel has a median depth of around 10 m, with maximum depth of
299
300 160 approximately 30 m (Gupta et al., 2007).

301 161 The field survey was conducted for 8 days, from 26 June to 2 July 2017, at the beginning of
302
303 162 the wet season. There were neither extreme floods nor low water situations, thus the
304
305 163 hydrodynamic conditions were suitable for sampling and analysing a typical (median)
306
307 164 suspended sediment distribution in the river. Twenty-seven samples were taken in the main
308
309 165 Mekong river and its tributaries (Nam Ou, Nam Suang and Nam Khan tributaries). During the
310
311 166 survey, hydro-sedimentary conditions were also characterized on two cross-sections with
312
313 167 distances of approximately 20 km (Fig. 1a, see section 2.2.3). For each location, samples were
314
315 168 collected in three vertical profiles (left bank – V1, middle bank – V2 and right bank – V3). In
316
317 170 each vertical profile, 3 litres of water sample were taken at various depths (0.1 h, 0.4 h, 0.7 h
318
319 and 0.9 h, h being total water depth).

318 171 2.1.2. Lacustrine environment

320
321 172 With volume of 1.8 – 58.3 billion m³, the Tonle Sap lake is the largest freshwater source in
322
323 173 Southeast Asia (Kummu et al., 2014). It is located in the Cambodian floodplain (Fig. 1c) and
324
325 174 comprises a permanent waterbody, twelve tributaries, extensive floodplains and the Tonle Sap
326
327 175 river linking the lake to the Mekong river (Kummu et al., 2014). At the confluence, the river
328
329 176 splits into the Bassac river (Hau river) in the West and the Mekong river (Tien river) in the
330
331 177 East. The Tonle Sap system has strong and original hydrodynamic relationships with the
332
333 178 Mekong mainstream (Kummu et al., 2008). During the wet season, flooding from the Mekong
334
335 179 river causes a reverse flow direction, into the Tonle Sap lake. The lake area then increases
336
337 180 from 2500 km² to approximately 15000 km², while the depth rises from 1 to 9 m. At the
338
339 181 opposite, the slow release of floodwaters from the lake during the dry season is a very
340
341 182 important water source to sustain the river discharge of the Mekong delta (Hai et al., 2008). In
342
343 183 this specific paper, we focus on the physics of particles. The field survey was performed for 9
344
345 184 days from 13 October to 21 October 2018, during high flow season. The material used is
346
347 185 freshly deposited sediment, collected near the Mekong river tributaries, after a flood season at
348
349 186 the bottom layer.

345 187 2.1.3. Estuarine environment

347
348 188 The Mekong delta (MD) is situated at the most Southeast part of the LMR (Fig. 1d). It covers
349
350 189 approximately 55,000 km² (Balica et al., 2014), extending from the Cambodia - Vietnam
351
352 190 border to the Gulf of Thailand and the East Sea of Vietnam (Tran et al., 2018). Together with
353
354

355
356
357
358
359
360
361
362
363
364
365
366
367
368
369
370
371
372
373
374
375
376
377
378
379
380
381
382
383
384
385
386
387
388
389
390
391
392
393
394
395
396
397
398
399
400
401
402
403
404
405
406
407
408
409
410
411
412
413

191 the Mekong river and the Bassac river, it separates into eight tributaries (Hung et al., 2014)
192 before discharging into the East Sea (Wolanski et al., 1996 and Xing et al., 2017). At the
193 interface between land and the sea, the estuary is strongly impacted by both flooding from
194 upstream and the tidal flows, as well as wave forcing (Gugliotta et al., 2019).

195 Three surveys with contrasted seasonal conditions were conducted in the Song Hau estuary
196 (as part of the Lower Mekong Delta Coastal Zone project), in December 2015, March and
197 October 2016. During these surveys, three cross-sections (upstream - T1, middle - T2,
198 downstream - T3), with distances of 10 and 15 km, respectively, were chosen to monitor and
199 assess the impact of saline water intrusion on flocculation (Fig. 1d and sketch of Fig.6). At
200 each location, samples were taken in three vertical profiles. In total, 104 samples with volume
201 of 5 litres per sample were collected to investigate the spatio-temporal dynamics of suspended
202 sediment for contrasted sediment concentration (SSC) and turbulent levels.

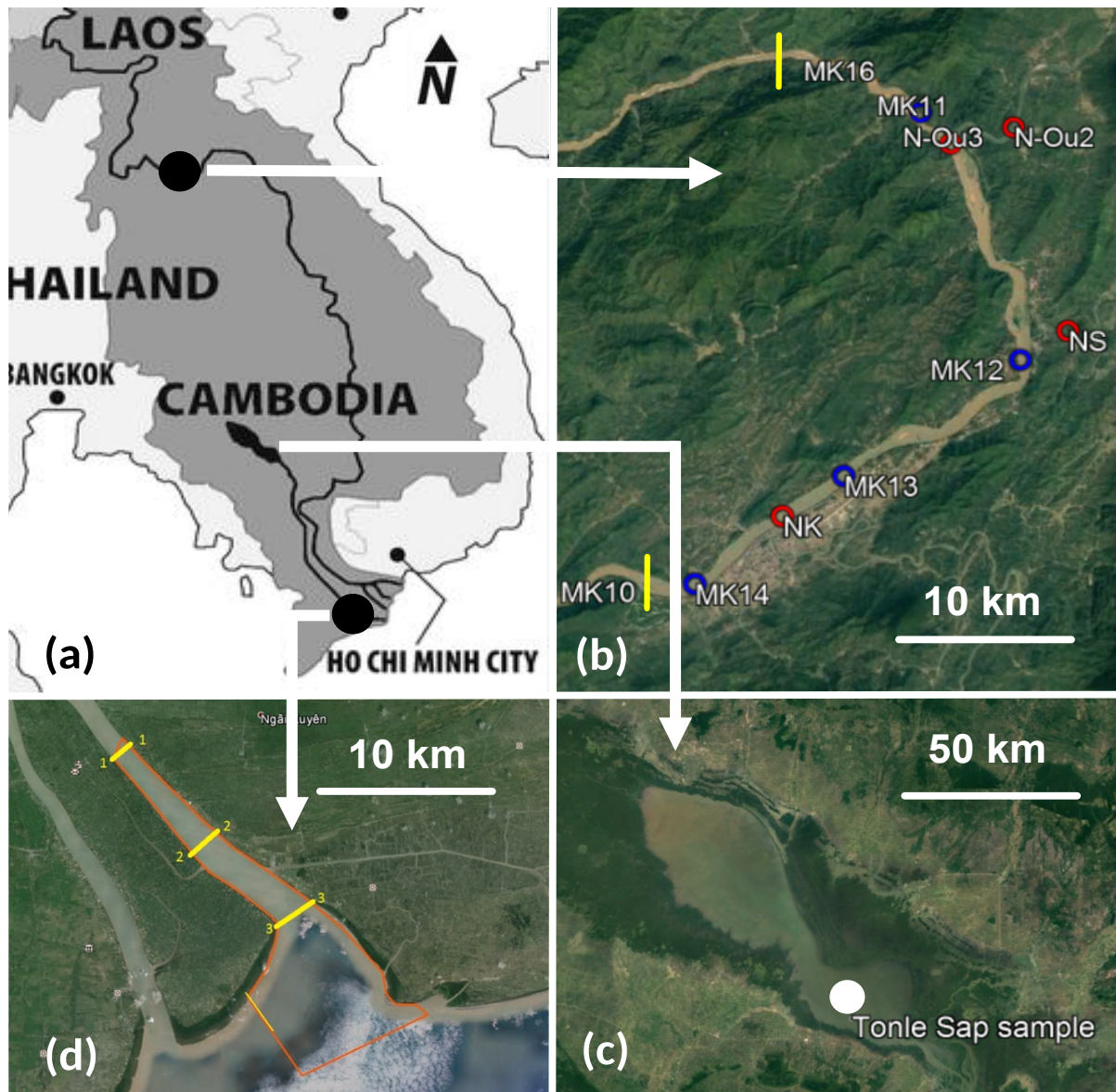


Fig. 1. Domains of interest [a] (Smardon et al., 2009). Sampling sites and locations in fluvial (Luang Prabang, Laos with blue dots reporting samples in main stream, red dots reporting samples in tributaries and yellow segments reporting cross-sections [b]), lacustrine environment (Tonle Sap floodplain, Cambodia with white dots showing the sampling location [c]), and estuarine environment (Song Hau estuary, Vietnam with yellow segments reporting cross-sections and red lines showing the local domain [d]).

2.2. Methods

The suspension regime of the sediments transported in a flow strongly depends on interactions between hydrodynamics, particle size, density and settling velocity. Thus, the understanding of particle size distribution (PSD) of suspended particulate matter (SPM) is one of prerequisites to properly simulate sediment dynamics (Fennessy et al., 1994). This study

473
474
475
476
477
478
479
480
481
482
483
484
485
486
487
488
489
490
491
492
493
494
495
496
497
498
499
500
501
502
503
504
505
506
507
508
509
510
511
512
513
514
515
516
517
518
519
520
521
522
523
524
525
526
527
528
529
530
531

215 originally proposes a direct estimation of settling velocity and flocculation with the patented
216 SCAF instrument (System for the Characterization of Aggregates and Floccs, Gratiot et al.
217 2015).

218 The five sections hereinafter describe the methodology adopted to measure the physical
219 properties of suspended sediment and evaluate its transport dynamics. The instruments at our
220 disposal are particularly relevant to estimate both particle size and settling velocity, but it was
221 not possible to measure directly the density of floccs, which may be seen as a limitation.

222 2.2.1. A portable mixing tank device to reproduce natural inflow turbulent conditions

223 To measure PSD under turbulent conditions close to the ones experienced by natural rivers, 2
224 litres of water samples were introduced into a portable rectangular-base mixing jar tank (with
225 diameter of 11.5 x 11.5 x 15 cm), and then mixed with an impeller for thirty minutes. Since
226 the work of Gratiot and Manning (2004), this mixing duration is assumed to ensure a good
227 homogenization of the fluid mud mixture, and a dynamic equilibrium between the rate of
228 flocculation and breakage. Some details on the experimental set-up can be found in Gratiot et
229 al. (2017). During preliminary experiments, an Acoustic Doppler Velocity Profiler (Nortek
230 Vectrino2) was immersed in the mixing tank filled with clear water, in order to measure
231 the 3D turbulent field of velocity and deduce the mean turbulent energy dissipation rate G (s^{-1}).
232 With a rotation speed of 100 rpm, G was about $44 s^{-1}$, which corresponds to high shear rate
233 conditions, such as observed near bottom in natural rivers and estuaries (Gratiot et al., 2017).
234 For further details on the mixing tank device, the reader can refer to Gratiot et al. (2017,
235 supplementary information).

236 2.2.2. PSD measurements and characterization of the particle-classes/population/group?

237 To characterize the different populations of particles, the terminology of Lee et al. (2012) is
238 used. It is based on four classes, namely primary particles, flocculi, microflocs and macroflocs
239 (as mentioned in the Introduction section). We utilize the LISST-Portable XR instrument to
240 measure sediment particle sizes during mixing. The operational principle of the LISST-
241 Portable XR is based on laser light scattering (or laser diffraction). This instrument provides
242 the logarithmical PSDs over 44-size bands in the ranges of particle size from 0.35 to 500 μm
243 by using the Fraunhofer approximation or the exact Lorenz-Mie theory. The volumic
244 concentration is in micro-litre/litre ($\mu L.L^{-1}$), corresponding to sediment concentration of 30 -
245 1900 $mg.L^{-1}$ in the chamber of measurement. Each spectrum shows independent semi-log
246 distributions of sub-populations, that were characterized by their mean particle size D_f , their

532
533
534
535
536
537
538
539
540
541
542
543
544
545
546
547
548
549
550
551
552
553
554
555
556
557
558
559
560
561
562
563
564
565
566
567
568
569
570
571
572
573
574
575
576
577
578
579
580
581
582
583
584
585
586
587
588
589
590

247 standard deviation σ_{Df} and their relative volumetric concentration. The operating range of
248 optical transmission recommended by LISST-Portable XR is 75 - 95 %. For optical
249 transmission lower than 75 %, multiple-scattering can bias the signal and lead to an
250 underestimation of the size distribution.

251 This device has been utilized successfully in many contrasted environments, such as the
252 Saigon - Dong Nai rivers, Vietnam (Nguyen et al., 2019), a hydropower plant in Malaysia
253 (Azrulhisham et al., 2018), Northern French Alps (Antoine et al., 2015) and Philadelphia
254 (Windt et al., 2017), among others.

255 It is worth noting that many other techniques exist to measure PSD, particularly video-based
256 techniques, such as the immersed INSSEV instrument (Fennessy et al., 1994) or the LabFlocs
257 portable video system (Manning et al., 2007). All methods have advantages and
258 disadvantages, so that a combination of different techniques is probably the best efficient.

259
260 For describing PSDs of primary particles, flocculi, microflocs and macroflocs, we apply a
261 mathematical function to separate the signal into four log-normal distribution (Mikkelsen et
262 al., 2006). Such post processing is also useful to prevent misinterpretation, resulting from air
263 bubbles and other artefacts that can be observed in the raw particle size spectrum (Sequoia,
264 2016).

265 In this study, the PSD of each sample was measured in two steps, before and after two
266 minutes of sonication, for a mechanical particle breakage under acoustic waves. Hence, it is
267 possible to assess the proportion of sand and flocs because large-size particles built by smaller
268 cohesive particles (silt or clay) are, at least partially, dispersed by sonication (Gratiot et al.,
269 2017) while the sand particles are indivisible and then maintain a constant diameter after
270 sonication.

271 2.2.3. Characterization of the settling and flocculation regimes

272 Depending on SSC, three settling regimes can be observed for natural sediment in aquatic
273 environment (Van Leussen, 1994), namely (1) free settling, (2) flocculation and (3) hindered
274 regimes. For the lowest SSC, flocculation is weak and particles are settling almost
275 independently from each other (free settling regime). Particle settling velocity can then be
276 broadly estimated by the Stokes' law or derived laws as the sum of individual particles
277 settling down (Stokes, 1857; Winterwerp, 2002). The flocculation settling regime occurs with
278 midrange of SSC (tens to hundreds of mg.L^{-1}). The settling velocity of cohesive and mixed
279 fine-grained sediments then becomes more complex because it is influenced by both particle

591
592
593 280 interactions and individual properties (Manning et al., 2010), as well as turbulent shear
594
595 281 (Winterwerp, 2002; Manning et al, 2011a). Flocculation is promoted, which results in larger
596
597 282 particle sizes and higher settling velocities (Droppo et al., 2005). The hindered settling regime
598
599 283 occurs at very high SSC (several grams per litre or more), and settling mostly occurs by mass,
600
601 284 depending on the cohesion and suspension concentration (Camenen and Van Bang, 2011; Van
602
603 285 and Van Bang, 2013).

604 286 To assess the settling velocity w_s ($\text{m}\cdot\text{s}^{-1}$) (and flocculation) for all these regimes in natural
605
606 287 environment, we used the System for the Characterization of Aggregates and Flocs (SCAF), a
607
608 288 recently patented instrument (Gratiot et al., 2015) that was successfully applied in some recent
609
610 289 researches (Wendling et al., 2015, Gratiot et al., 2017, Legout et al., 2018, Nguyen et al.,
611
612 290 2019). This instrument is a glass settling column with dimension of 20 cm high and 3.5 cm in
613
614 291 diameter, equipped with 16 infrared ($\lambda = 980$ nm) emitters and 16 diametrically opposed
615
616 292 photo-sensors measuring at a frequency of 210 Hz. SCAF instrument measures the light
617
618 293 attenuation in the settling tube with depth and time during the deposition of particles (Gratiot
619
620 294 et al., 2015). Sensors are located every 1 cm down the column with the lower sensor located at
621
622 295 1 cm above the bottom of the column. Measurements taken in the eight upper centimeters of
623
624 296 the SCAF settling tube provided an estimate of flocs settling velocity under quiescent
625
626 297 conditions, denoted $w_{s,q}$ ($\text{m}\cdot\text{s}^{-1}$) while measurements realized in the eight centimetres near the
627
628 298 bottom of the settling tube provided an estimation of flocs settling velocity after flocculation
629
630 299 by differential settling under settling dominated conditions, this latter velocity being reported
631
632 300 as $w_{s,\neq}$ (Wendling et al., 2015). In the case of non-cohesive particles, such as sand or silt, or
633
634 301 clay particles with deflocculant, the settling velocity does not change during settling; $w_{s,q}$ and
635
636 302 $w_{s,\neq}$ are similar and the flocculation index $\text{FI} = (w_{s,\neq} - w_{s,q}) / w_{s,q}$ is close to zero (Wendling et
637
638 303 al., 2015). As SCAF instrument is based on by mass sedimentation of a fluid mud mixture in a
639
640 304 settling tube, it is inherently affected by the shape, density and compositions of all particles
641
642 305 presented in the sample.

636 306 2.2.4. Other hydrodynamic measurements

639 307 Complementary measurements were performed during field surveys. An Acoustic Doppler
640
641 308 Current Profiler (ADCP), an Hydrolab probe (a multi-parameter probe measuring in-situ
642
643 309 water quality parameters), SSC samplers and a EUTECH turbidimeter were used to
644
645 310 characterize the water flow in the cross-sections, suspended solid concentration and physical
646
647 311 parameters such as turbidity, temperature, pH, ORD, EC, salinity, etc. An YSI multi-

650
651
652 312 parameter probe (Water Quality Sampling and Monitoring Meters and Instruments) was also
653
654 313 used to check the average values of the measured physical parameters.

655 656 314 2.2.5 Characterization of the suspension regime

657
658
659 315 In order to characterize the suspension regime, the non-dimensional Rouse number (Rouse,
660 316 1937), which express the balance between the upward turbulence forces (u_*) lifting the
661
662 317 particles and the gravity forces applied (w_s) on the same particles in a river stream, was
663
664 318 calculated for each flow condition encountered. The Rouse number is calculated as following:

$$665
666
667 319 \quad R_o = \frac{w_s}{\beta \kappa u_*} \quad (1)$$

668
669
670 320 where the settling velocity w_s is inferred from the SCAF results (Fig. 5), or calculated by the
671
672 321 Stokes' Law from the PSD measurements. κ is the von Kármán constant, taken equal to 0.41.
673
674 322 The constant of proportionality β is the ratio of sediment to eddy diffusivity, describing the
675
676 323 diffusion patterns of a fluid particle and a sediment particle. In water environment, it is often
677
678 324 assumed that eddy viscosity is equal to eddy diffusivity, thus value β is typically
679
680 325 hypothesised to be one (Rijn, 1984; Farrell and Sherman, 2013). u_* (m.s^{-1}) is shear velocity.
681
682 326 In the fluvial and estuarine environments, the shear velocity u_* was computed by using the
683
684 327 ADCP, with the assumption that the velocity profiles follow the logarithmic inner-law (so-
685
686 328 called "Law of the Wall") (Sime et al., 2007; Santini et al., 2019, Eidam et al., 2017). In the
687
688 329 lacustrine environment, u_* was computed from 2D hydrodynamic simulation results by the
689
690 330 Second-generation Louvain-la-Neuve Ice-ocean Model (SLIM, <https://www.slim-ocean.be/>).

691
692 331 The application of Eq.1 to characterize the suspension regime is relevant, but we should
693
694 332 underline that uncertainties can be high, as both w_s and u_* are hardly estimate in the field.

695 696 333 **3. Results**

697 698 334 *3.1. Particle size distribution (PSD)*

699
700 335 The PSD of all samples are gathered in a triangle sketch in Fig. 2. Before sonication, most of
701
702 336 the particles are flocculi with an average contribution percentage of 46 %, 78 % and 78 %, for
703
704 337 fluvial, lacustrine and estuarine environments, respectively (Fig. 2a). After sonication, the
705
706 338 PSD displayed an increased number of primary particle class for all samples (51 %, 67 % and

709
710
711
712
713
714
715
716
717
718
719
720
721
722
723
724
725
726
727
728
729
730
731
732
733
734
735
736
737
738
739
740
741
742
743
744
745
746
747
748
749
750
751
752
753
754
755
756
757
758
759
760
761
762
763
764
765
766
767

339 32 %, respectively), while it witnessed the reduction in the percentage of flocculi and flocs
340 (Fig. 2b). This figure also shows a wider diversity of particle sizes in the Mekong estuary
341 (blue circles and squares) than in the lacustrine and the fluvial environments (yellow and red
342 circles, respectively). It illustrates that estuaries are complex and changing environments,
343 which mix both fluvial and coastal water (see the sketch in Fig.6 and the corresponding
344 discussion section). In the case of the Mekong estuaries zone, sediment transport and
345 deposition is strongly affected by fluvial inflow, tidal currents, but also resuspension of
346 particles by wind-induced current, waves and coastal oceanic currents (Gugliotta et al., 2019;
347 Marchesiello et al., 2019).

768
769
770
771
772
773
774
775
776
777
778
779
780
781
782
783
784
785
786
787
788
789
348
791
792
349
793
794
795
796
797
798
799
800
801
802
803
804
805
806
807
808

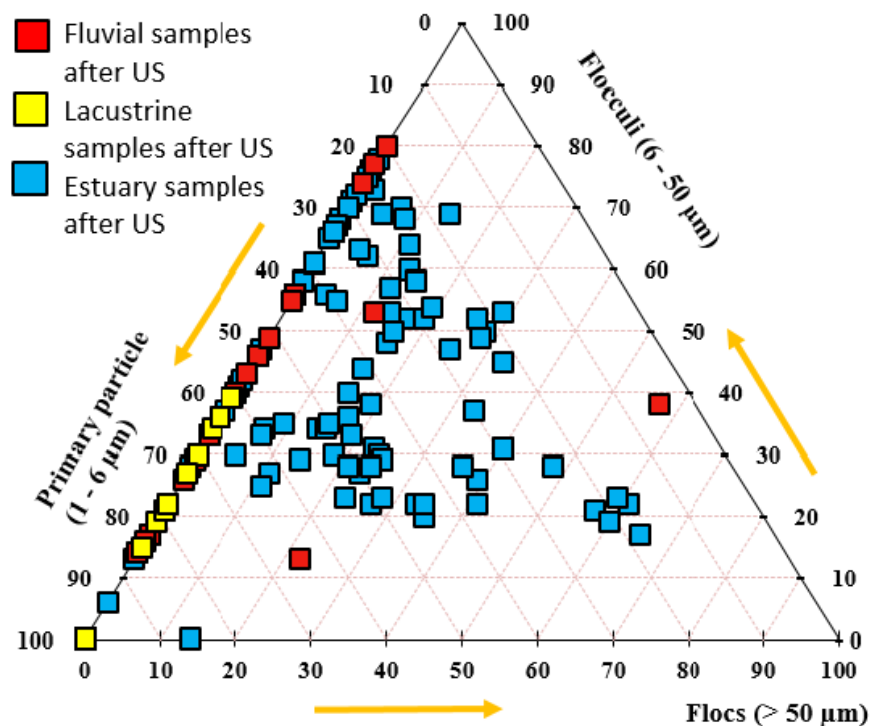
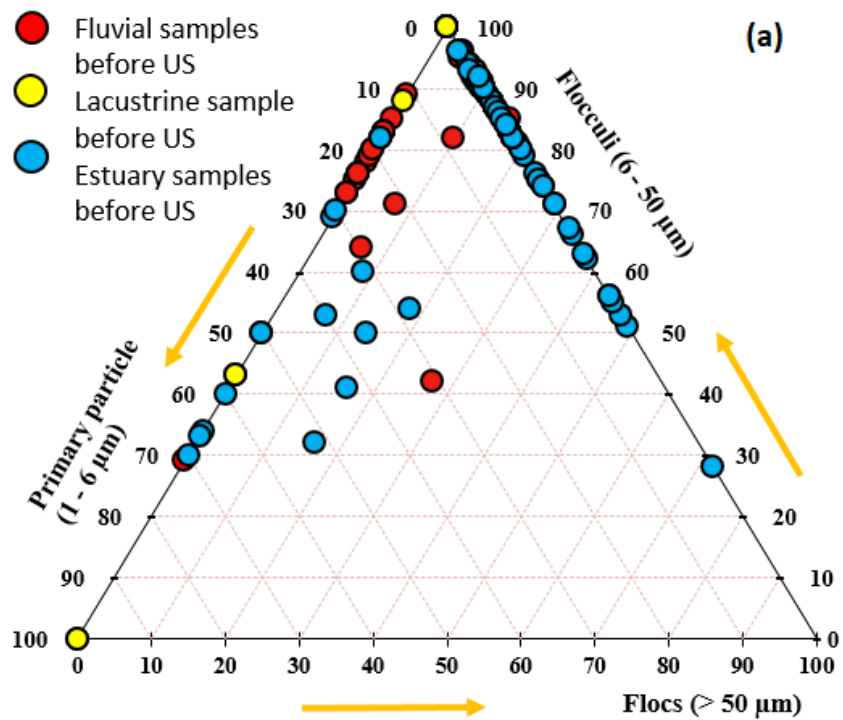
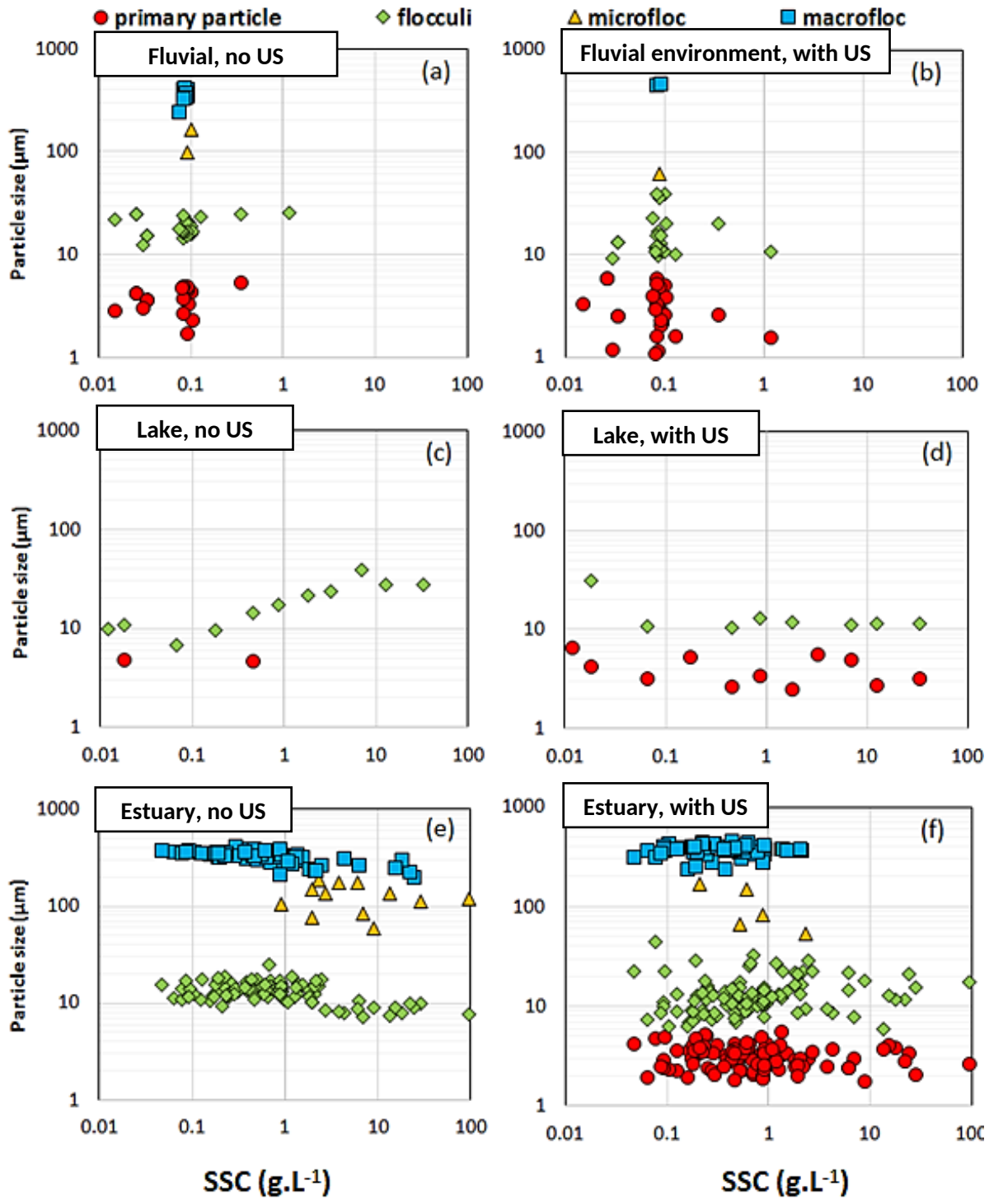


Fig. 2. Triangulars of PSD in upper parts and estuary analyzed (a) before and (b) after sonication

809
810
811
812
813
814
815
816
817
818
819
820
821
822
823
824
825
826
827
828
829
830
831
832
833
834
835
836
837
838
839
840
841
842
843
844
845
846
847
848
849
850
851
852
853
854
855
856
857
858
859
860
861
862
863
864
865
866
867

350 3.2. Suspended sediment versus hydrodynamic conditions

351 Fig. 3 aims at highlighting the role played by SSC on flocculation of particles. This figure
352 gathers both data collected in the field and in the laboratory, before and after sonication.



353
354 **Fig. 3.** Variation of particle classes with SSC in fluvial environment, lacustrine environment
355 and estuary before and after sonication

868
869
870 356 3.2.1. Particle size populations in the fluvial environment (Laos)
871

872
873 357 Fig. 3 (a) and Fig. 3 (b) present the PSD of particles populations sampled in the fluvial
874 358 section. On average, the primary particles accounted for 37 % of all particle population (in
875 359 volumetric concentration). The predominant population is flocculi, with a volume
876 360 concentration of approximately 46 %. Microflocs and macroflocs were fewer and accounted
877 361 for (only) 3 % and 14 % of the total volume, respectively. The macroflocs size reached a
880 362 median diameter of 422 μm . Fig. 3 (b) shows the PSD plot after sonication. The sonication
882 363 broke up particles so that the percentage of primary particles increased (+14 %) to 51 % and
883 364 flocculi decreased slightly (-5 %) to 41 %. The percentage of microflocs remains stable and
885 365 small (approximately 2 %), and the percentage of macroflocs decreases by more than two
887 366 folds (to approximately 6 %). These coarsest particles were not all broken up by sonication,
888 367 which indicates the presence of sand. The samples issued from the tributaries had generally
890 368 similar PSDs than the ones in the mainstream. After sonication, PSD of these samples still
892 369 exhibits high values, with a maximum diameter of 347 μm . It means that these water samples
893 370 contains predominantly sand, which is in agreement with visual observations during field
894 371 campaigns. A detailed examination of PSD before and after sonication confirmed that samples
896 372 in fluvial environment consisted of both cohesive sediment and sand particles. These PSDs
898 373 are in agreement with the results of Camenen et al. (2014).

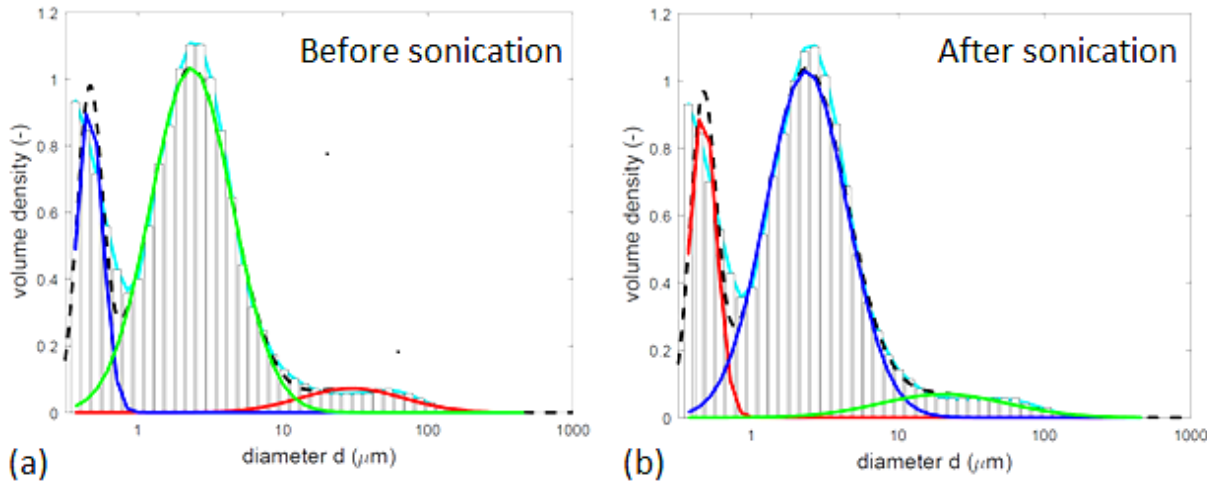
900
901 374 3.2.2. Particle size populations in the lacustrine environment (Tonle Sap, Cambodia)
902

903 375 In the lacustrine environment, only two particles classes (primary particles and flocculi,
904 376 without flocs and no sands) appear. Before sonication (see Fig. 3c), the percentage of primary
905 377 particles and flocculi accounts for 22 % and 78 %, respectively. After sonication (see Fig. 3d),
907 378 these percentages reverse with a predominance of primary particle (67 %) and a simultaneous
909 379 decrease of flocculi (33 %). The particle size in the lacustrine environment were smaller ($7 \pm$
911 380 $3 \mu\text{m}$) than in the fluvial part ($18 \pm 5 \mu\text{m}$). Fig. 3c exhibits a clear rise (3 to 4 folds) of flocculi
912 381 size with higher SSC, as a response of flocculation of primary particles (or colloids) on
914 382 flocculi.

916
917 383 Interestingly, colloids were observed in some samples taken in the Tonle Sap, with diameters
918 384 of $< 1 \mu\text{m}$ (see Fig 4). After 12 hours of deposition in the mixing tank at rest, the particles still
919 385 in suspension were both colloids with diameter of approximately 0.45 μm , which are
920 386 consistence with a research conducted by Seah et al 2017, accounting for 21 %; primary
921
922
923
924
925
926

927
928
929
930
931
932
933
934
935
936
937
938
939
940
941
942
943
944
945
946
947
948
949
950
951
952
953
954
955
956
957
958
959
960
961
962
963
964
965
966
967
968
969
970
971
972
973
974
975
976
977
978
979
980
981
982
983
984
985

387 particle (73 %) and few flocculi (6 %). After sonication, the structure of sediments presents
388 the same pattern (21 % of colloid, 72 % of primary particles and 7 % of flocculi). This can be
389 explained by a stable mixture of this sediment classes, which are hardly broken down into
390 smaller particles even after sonication. Colloids play an important role and act as “catalyzers”
391 of the interaction between sediment and substances in the water such as substance dissolved
392 matter, substance from precipitation, absorbed ions and organic matters (Wendling et al.,
393 2015).



394
395 **Fig 4.** PSD of a sample in the Tonle Sap before (a) and after sonication (b). The first peaks in
396 two graphs show the appearance of colloids with diameter of < 1 μm.

397 3.2.3. Particle size populations in the estuarine environment (Song Hau river, Vietnam)

398 Fig 3 (e and f) display the PSD in the estuary versus SSC before and after sonication,
399 respectively. Once again, flocculi is the dominant population of particles, with mean diameter
400 of approximately 15 μm (in range of 8 - 20 μm), accounting for 80 % of total volume. Before
401 sonication, only three classes of particle sizes exist in the estuarine samples, flocculi,
402 microflocs and macroflocs. The prevailing fine silt population shows mean diameter of 7 –
403 12.5 ± 10 % μm, that constituted 83 – 94 % of total volume. Diameters of coarser population
404 were in the range of 112 – 310 ± 10 % μm. After sonication, particle size reduced
405 significantly. A group of primary particles (red circles), which were completely absent from
406 the PSDs before sonication, appears in almost all samples, which undoubtedly demonstrates
407 the cohesive nature of sediments in the estuary. Due to breakage into smaller particles under
408 turbulence shear, diameters of fine particles (primary particles and flocculi) reduce to 1.8 – 4
409 ± 10 % μm and 6.3 – 12.2 ± 10 % μm, respectively while the size of coarse particle

986
987
988 410 (microflocs) falls to $15 - 65 \pm 10 \text{ } \mu\text{m}$. A population of sand particles (with diameter > 200
989 411 μm), not broken-up with/after sonication, is also evidenced.

992 412 3.3. *Settling velocity*

993
994
995 413 Fig. 5(a) shows the variation of suspended sediment settling velocity with SSC, measured
996 414 directly with SCAF instrument. For the three aquatic environments, settling velocity rises with
997
998 415 SSC because of flocculation process. Even if there are only 5 SCAF samples in the fluvial
999
1000 416 environment, 9 samples in lacustrine environment, 19 samples in the estuary, the three curves
1001 417 exhibit similar trends, which support the existence of free settling, flocculation and hindered
1002
1003 418 regimes, as previously depicted by Wendling et al. (2015).

1004
1005 419 The free settling regime is observed for the lowest SSC (tens of mg.L^{-1}). Sediment settling
1006
1007 420 velocity measured in the fluvial, lacustrine and estuarine environments are of the same order
1008
1009 421 of magnitude, the mean settling velocities being approximately $0.02 - 0.08 \text{ mm.s}^{-1}$ in the
1010 422 fluvial section, $0.05 - 0.06 \text{ mm.s}^{-1}$ in the lake, and $0.01 - 0.02 \text{ mm.s}^{-1}$ in the estuary. The
1011
1012 423 widest range of settling velocities observed in the fluvial environment is probably the
1013 424 fingerprinting of a wide variety of compact soil aggregates, freshly eroded from the
1014
1015 425 watershed, and not yet at equilibrium with the prevailing hydrodynamic conditions, as
1016
1017 426 reported conceptually by Droppo et al. (2015). In this free settling regime, particles settle
1018 427 almost independently, the interaction between particles is poor, which is reflected by a
1019
1020 428 moderate flocculation index (FI lower than 2) in all SCAF measurements (in Fig. 5, right
1021 429 panel). Flocculation predominates in the range of $0.4 - 4 \text{ g.L}^{-1}$, thus the settling velocities of
1022
1023 430 fluvial, lacustrine and estuarine sediments rise up to 0.2 mm s^{-1} , $0.1 - 2 \text{ mm.s}^{-1}$ and $0.03 - 0.8$
1024
1025 431 mm.s^{-1} , respectively.

1026
1027 432 In the lacustrine environment, a significant rise of settling velocity is found with higher SSC.
1028
1029 433 The SCAF results show that the settling velocity of the lacustrine environment reaches the
1030 434 peak of 2.0 mm.s^{-1} when SSC reach approximately 2.0 g.L^{-1} .

1031
1032
1033 435 In the estuary, the complex hydraulic regimes, including resuspension of freshly deposited
1034 436 sediments (Marchesiello et al., 2019) and the mixing between fresh water and saline water led
1035
1036 437 to the formation of a zone of turbidity maximum and promote the formation of flocs (both
1037
1038 438 microflocs and macroflocs) (Dyer et al., 2002a and Manning et al., 2007). As a consequence,
1039 439 the settling velocity also increases (Dyer et al., 2002b and Manning et al., 2011b). Beyond 4.0
1040
1041 440 g.L^{-1} , hindered regime becomes predominant. It implies the decline of settling velocity in the

1045
1046
1047 441 lacustrine and estuarine environments, from 2.0 to 0.4 mm.s⁻¹ and from 0.8 to 0.1 mm.s⁻¹,
1048
1049 442 respectively.

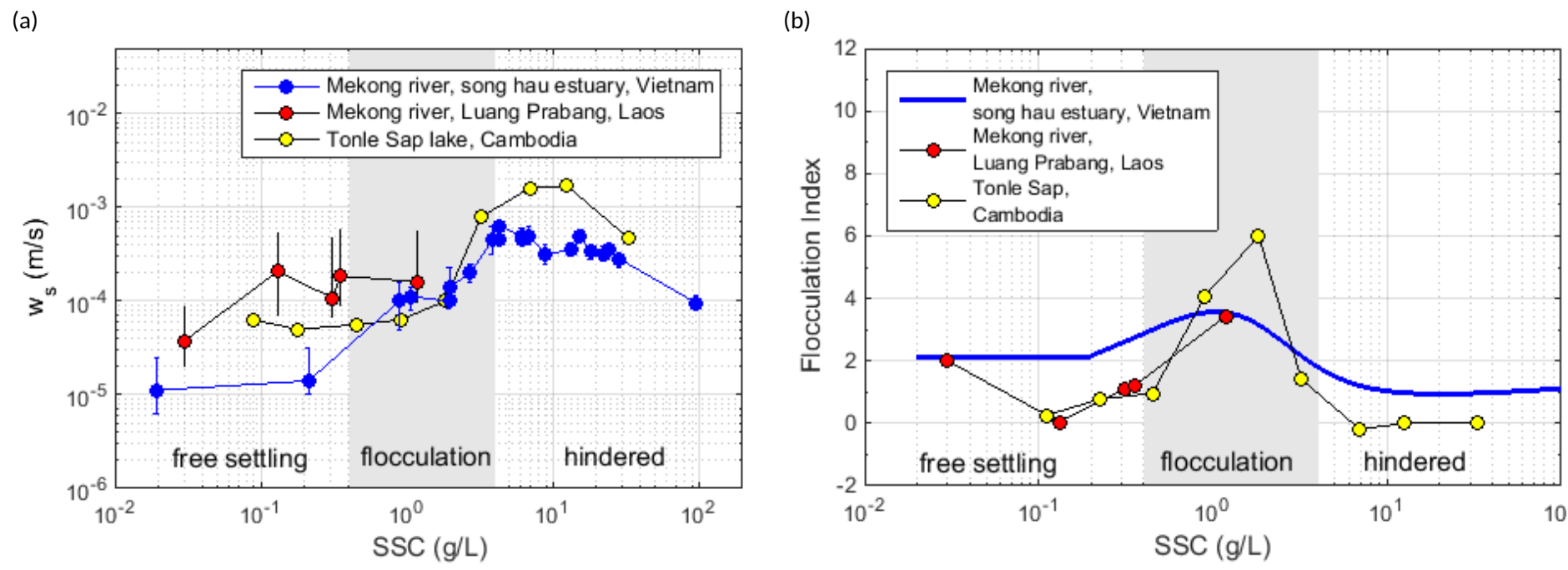
1050
1051 443 The main difference of these three environments is that flocculation processes seem to appear
1052
1053 444 at lower concentration in the fluvial environment (approximately 20 - 30 mg.L⁻¹) than in the
1054
1055 445 lake (approximately 1 - 2 g.L⁻¹) or in the estuary (approximately 300 mg.L⁻¹). We cannot
1056
1057 446 exclude that the particles sampled in the fluvial environment are not real flocs, but correspond
1058
1059 447 to soil aggregates that are not in equilibrium with their hydraulic environment (Droppo et al.,
1060
1061 448 2005).

1062 449 The flocculation efficiency is higher for the estuarine environment (+ 60 % of increase of the
1063
1064 450 settling velocity) and highest for lacustrine environment (+200 % of increase) than for the
1065
1066 451 fluvial environment (+7 % of increase).

1067 452 Concerning the Flocculation Index (FI), sediment samples in the river and in the lake (red
1068
1069 453 circles for fluvial environment and yellow circles in lacustrine environment, see Fig. 5b)
1070
1071 454 exhibit a high dynamic, even in fresh water. The highest rate of flocculation is observed in the
1072
1073 455 lacustrine environment, where the measured FI increases from 0 to 6, when SSC increases
1074
1075 456 from 0.1 to 3.0 g.L⁻¹. Interestingly, after getting the FI peak of 4 – 6, the efficiency of
1076
1077 457 flocculation in the lacustrine environment fell to value of 0 – 1.75. It means that flocculation
1078
1079 458 still occurs, but the volumetric concentration of particles is so high that the settling velocity
1080
1081 459 cannot increase anymore. Settling velocity of small particles is hindered by the high SSC,
1082
1083 460 whereas colloids are trapped on the surface of larger particles (Comba et al., 2009).

1082 461 The estuarine sediments also experience three settling regimes with FI in range of 0 - 3: (1)
1083
1084 462 Free settling regime with constant FI of 2, that is developed at low concentration of 300 mg.L⁻¹;
1085
1086 463 (2) Flocculation regime with FI < 3, where flocculation happens at SSC of 300 - 2700 mg.L⁻¹;
1087
1088 464 (3) Hindered regime with FI of approximately 1 because of the appearance of brackish
1089
1090 465 water and high SSC of > 2.7 g.L⁻¹. Flocs reach higher volumetric concentration for lower
1091
1092 466 mass concentrations when flocculation is reinforced by differential settling (Gratiot et al.,
1093
1094 467 2017).

1104
1105
1106
1107
1108
1109
1110
1111
1112
1113
1114
1115
1116
1117
1118
1119
1120
1121
1122
1123
1124
1125
1126
1127
1128
1129
1130
1131
1132
1133
1134
1135
1136
1137
1138
1139
1140
1141
1142
1143
1144



468 **Fig. 5.** Sediment properties in the Mekong Land to Ocean Continuum: (a) Variation of settling velocity with SSC measured directly with SCAF
469 instrument and (b) Variation of the flocculation index with SSC.

4. Discussion

4.1. Suspended sediment transport mechanisms along the Mekong

As mentioned in Section 2.2.4, the transport regime of suspended sediment along the LMR may be characterized through the non-dimensional Rouse number (R_o). For the upstream fluvial environment, the computed shear velocities were similar in the different sections monitored, $u_* = 0.03 \text{ m.s}^{-1}$ for the MK10 and $u_* = 0.04 \text{ m.s}^{-1}$ for MK16. The small difference between the two cross-sections may be explained by the geometry of each cross-section, MK10 cross-section being wider than MK16 cross-section. The shear velocity in the Tonle Sap is 0.008 m.s^{-1} by using SLIM simulation obtained by Le et al. (submitted); while a value of 0.010 m.s^{-1} is obtained by using the Inner law. The R_o values in the estuary are estimated based on two representative particle sizes ($15 \mu\text{m}$ for fine particles and $300 \mu\text{m}$ for sand) and the shear velocity is estimated with the recent work of Eidam et al. (2017).

The R_o values estimated for the fluvial, lacustrine and estuary environments are summarized in Table 1. In the fluvial environment, the R_o ranges between 0.002 and 0.009 at the two monitored river cross section (MK10 and MK16), which corresponds to the washload mode. Hence particles are presumably transported over long distances, without any interaction with the riverbed. Few sand particles are presents in the MK10 and MK16 cross section samples, with R_o values of 0.75 - 4.6. Its means that the very fine sand particles are strongly sorted over the water depth, leading to a low suspension mode. As for the coarser sand fraction of the riverbed, the stream was not able to transport them in suspension.

While R_o values of Tonle Sap samples vary from 0.005 – 0.015, corresponding to flow modes ranging from washload to strong suspension load (Vanoni et al., 1946 and Udo et al., 2011). It is assumed that sediments are deposited near bed during one part of the year, and eroded under wind-induced currents during another part of the year. According to Kumm (2008), the net budget of sediment is almost in equilibrium between deposition and erosion.

In the estuary, the value of the R_o for the fine sediments ranges between 0.007 - 0.058, which corresponds to strong suspension mode; while the values for sand vary from 2.4 to approximately 12, which corresponds to the bedload mode and sedimentation dominated regime (Gugliotta et al., 2019). This finding coincides with the recent study of Marchesiello et al. (2019) showing that the Mekong sediments consist of a mixture (fine sediments and sands)

under effects of complex forces. Thus coastal muds are exposed to wave-induced resuspension and wind-induced transport, while sands are concentrated near the estuaries.

Table 1. Ro value in two different conditions

Sample	Mean Diameter (μm)	u_* (m.s^{-1})		w_s (m.s^{-1})		Rouse value	
		Law of Wall	Modelled results	SCAF	Stokes' Law	Min	Max
Fluvial (MK10)	19 ± 2	0.029	-	2.0E-05	1.2E-04	0.002	0.009
Fluvial (MK16)	18 ± 4	0.041	-	8.0E-05	1.2E-04	0.005	0.007
Tonle Sap	7 ± 2	0.014	0.008	5.0E-05	2.0E-05	0.005	0.015
Estuary fine sediment	15 ± 2	-	0.01	3.0E-05	2.4E-04	0.007	0.058
Estuary sand	300 ± 30	-	0.02	2.0E-02	9.5E-02	2.439	11.6

4.2 Predominance of flocculi in the LMR and consequences for sediment transport

As quantified in this paper, flocculi is the dominant particles population in all three environments monitored at regional scale (46 % in the fluvial environment, 78 % in the lake and 78 % in the estuary). The existence of sand was noticed, but can mostly be found near the bed with few percent of volume.

In the Lower Mekong River as in many other large hydrosystems under tropical climates, we may anticipate that particles' populations (and its consequences) fluctuate seasonally and year after year. As designed, this study cannot catch these variations, however, we believe that it describes a general pattern that could be helpful when establishing some monitoring strategies in similar large tropical hydrosystems in South East Asia, and probably elsewhere. At large scale, Rouse analysis presented in Table 1 showed that particles are mainly transported with a strong suspension regime, evenly as washload by river flow. By these modes, they are transported abundantly along the main river and tributaries, partially over the floodplains during the flood season (Kondolf et al., 2014, Manh et al., 2014, Manh et al., 2015) and then, are deposited along shore and on the whole subaqueous delta, before having cycles of resuspension/deposition, principally under waves forcing (Marchesiello et al., 2019). Our measurements in the fluvial section show that few sands are transported in the water column because their transport, which do not flocculate, is completely governed by the stream power. During high flow with enhanced stream powers working with other sediment sources (riverbanks and floodplains), the finest sands are lifted into upper layer.

1263
1264
1265 523 This methodology can explain two distinct transport modes of two particles populations in the
1266
1267 524 Mekong estuary: washload is well mixed throughout the water column and sand are
1268
1269 525 transported prevailing near the bottom. It leads to distinct geomorphological forms, with the
1270 526 presence of alternated tidal flats and sand bars as observed in many river mouths (Ta et al.,
1271
1272 527 2002; Gupta et al., 2002; Anthony, 2015).

1274 528 *4.3. Occurrence of fluid mud layers in the Mekong estuary*

1275

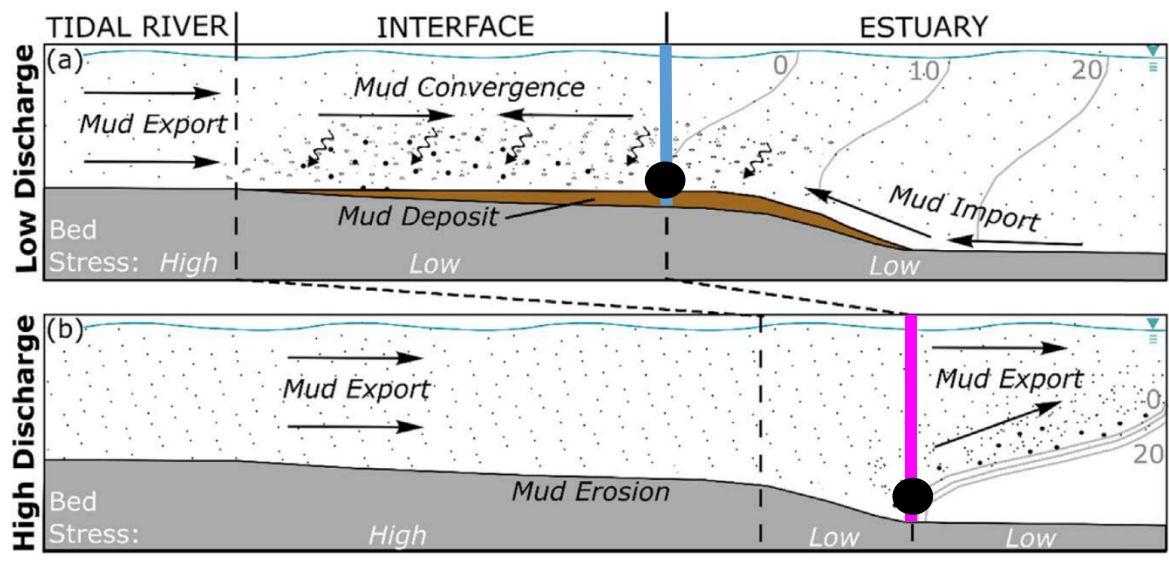
1276
1277 529 According to measured data during our three surveys in the estuary, a fluid mud layer was
1278
1279 530 sometimes formed near bottom, with SSC values abruptly increasing beyond 0.4 g.L^{-1} ,
1280 531 corresponding to the transition to the flocculation regime (Fig. 5; Gratiot et al., 2017). Fig. 6
1281
1282 532 sketches the sediment transport from the river to the estuary in low flow season (a) and high
1283 533 flow season (b) with locations of vertical profile sampling. In this figure, the blue profile
1284
1285 534 represents a schematic profile measured in low flow season and the purple one represents a
1286 535 profile measured in high flow season. Fig. 7 reports all SSC value observed near bottom ($z =$
1287
1288 536 $0.9h - SSC_{nb}$) for the vertical profiles realized in the estuary in December 2015 (50 profiles),
1289
1290 537 March 2016 (44 profiles) and October 2016 (47 profiles). Each vertical profile is represented
1291 538 by a single point in Fig. 7. The three curves show the sorted distribution of all SSC_{nb} values
1292
1293 539 for the three seasons. The curves show that the percentage of profiles which exhibits high SSC
1294 540 values, compatible with fluid mud layer occurrence, is very high during low flow season
1295
1296 541 (66 % of profiles in Dec 2015 and 95 % profiles in March 2016) and is much smaller during
1297 542 high flow season (9 % profiles in October 2016).

1298
1299
1300 543 By multiplying SSC_{nb} values with the corresponding settling velocity w_s , reported in Fig. 5, we
1301
1302 544 can estimate the settling flux capacity of fluid mud layers $\phi = SSC_{nb} \times w_s$ and thus assess
1303 545 their potential contribution to sedimentation (Fig. 7b). The cumulated sorted series
1304
1305 546 demonstrate the strong linearity between sediment concentration and settling flux (i.e.
1306
1307 547 potential of sedimentation). Fig.7c shows that the 10 % of the most concentrated fluid mud
1308 548 layers contributes to 60 % of the sedimentation during low flow season (blue curves) and
1309
1310 549 more than 98 % during high flow season (purple curve).

1311
1312 550 As a preliminary conclusion, our study confirms the existence of fluid mud layers and
1313
1314 551 quantifies broadly their frequency of occurrence in the estuary. Fluid mud layers are observed
1315
1316 552 within distances of approximately 30 km from the coastlines in both high flow and low flow
1317 553 seasons. However according to Wolanski et al. (1998), the location of fluid mud layer in the
1318
1319
1320
1321

1322
1323
1324
1325
1326
1327
1328
1329
1330
1331
1332
1333
1334
1335
1336
1337
1338
1339
1340
1341
1342
1343
1344
1345
1346
1347
1348
1349
1350
1351
1352
1353
1354
1355
1356
1357
1358
1359
1360
1361
1362
1363
1364
1365
1366
1367
1368
1369
1370
1371
1372
1373
1374
1375
1376
1377
1378
1379
1380

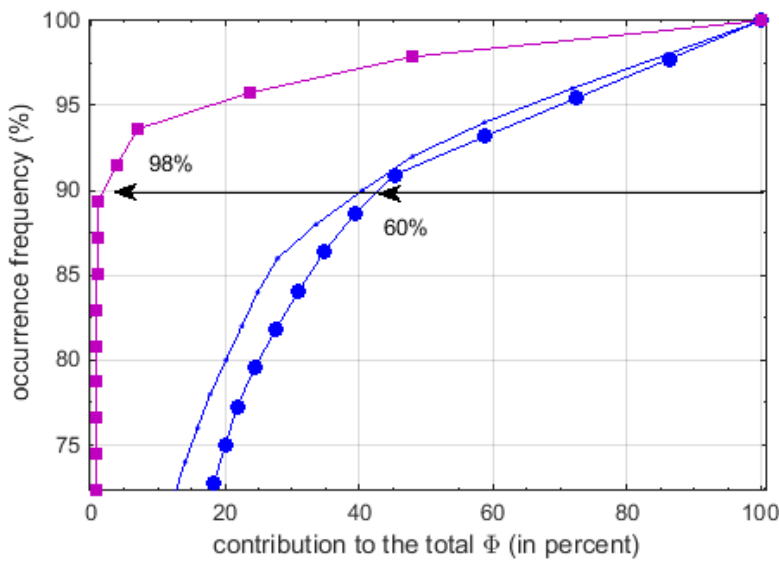
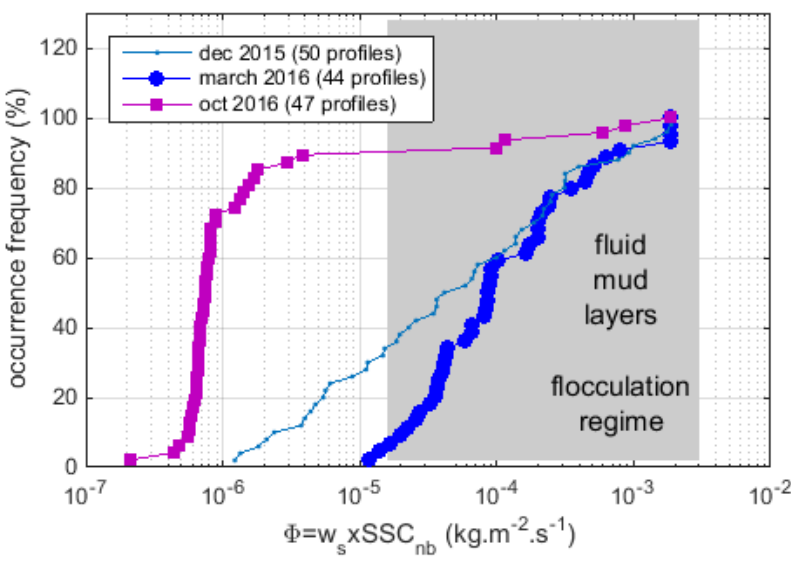
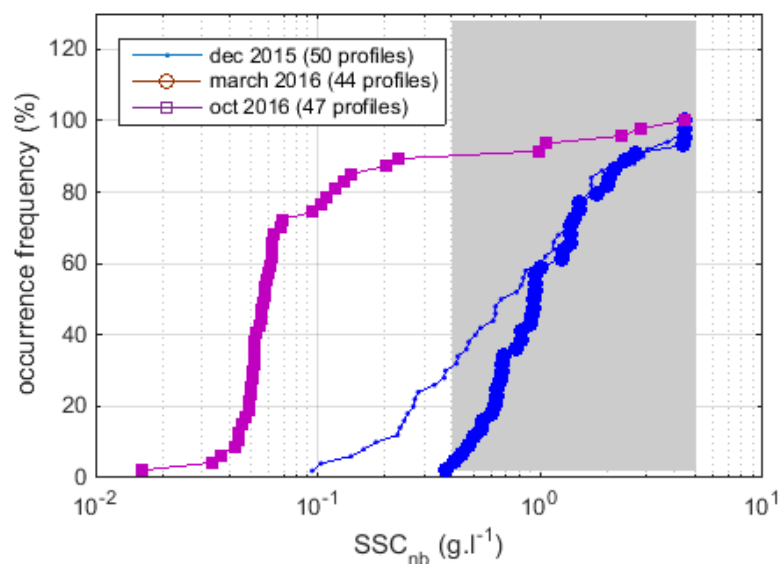
554 Mekong estuary varies spatially with river discharges and tides. In the high flow season, most
555 of sediment deposits in shallow coastal waters, approximately 10 - 20 km from the coast
556 (Wolanski et al., 1998 and Marchesiello et al., 2019). In low flow season, fine sediment is
557 well mixed with saline water penetrating about 40 km inland, carrying sediment up-river to a
558 turbidity maximum zone. Further upstream, at Can Tho, approximately 120 km from the
559 coast, no turbidity maximum is found in the freshwater region of the estuary. Thus the
560 positions of fluid mud layers and turbidity maximum, which are promoted by SSC
561 concentration in the range 0.4 - 4 g.L⁻¹, can hardly be observed for distances higher than 120
562 km inland. This situation could change in the future, under the cumulated effect of subsidence
563 and sea level rise.



564
565 **Fig 6.** Conceptual summary of salinity stratification (grey lines), SSC (dot concentration),
566 relative near-bed shear stress, suspended particle aggregation (dot size), net sediment
567 advection (black arrows), and mud deposition/erosion within the tidal river, tidal river –
568 estuary interface, and estuary during (a) low and (b) high discharge seasons. Relative weight
569 of transport arrows vary with season and regime. Not drawn to scale (after McLachlan et al.,
570 2017). The blue line shows the vertical profile in low flow season and the purple line shows
571 one in high flow season with SSC. The black dot shows the sampling height (near bottom, at
572 0.9 h).

573 According to Spearman and Manning (2008), the mass balance between accretion and erosion
574 of cohesive sediment during tidal cycles in estuarial location can occur when threshold shear
575 stresses for both deposition and erosion operate simultaneously.

1381
 1382
 1383
 1384
 1385
 1386
 1387
 1388
 1389
 1390
 1391
 1392
 1393
 1394
 1395
 1396
 1397
 1398
 1399
 1400
 1401
 1402
 1403
 1404
 1405
 1406
 1407
 1408
 1409
 1410
 1411
 1412
 1413
 1414
 1415
 1416
 1417
 1418
 1419
 1420
 1421
 1422
 1423
 1424
 1425
 1426
 1427
 1428
 1429
 1430
 1431
 1432
 1433
 1434
 1435
 1436
 1437
 1438
 1439



(a) **Fig 7.** Data corresponds to SSC measured near bottom (SSC_{nb}). Data are sorted from lowest to highest SSC (a), corresponding settling flux (b) and contribution to the total (c). The blue line shows the vertical profile in December 2015; the blue line with dots shows one in March 2016 and the purple line shows one in October 2016 with SSC near bed.

(c)

1440
1441
1442 576 *4.4. Implication for Mekong Delta management*
1443
1444

1445 577 In the MD, the flocculation process plays an essential role in the formation of fluid mud layer
1446 578 by enhancing the downward flux of sediment when freshwater mixes with seawater and
1447 579 sediments become trapped at the convergence point. Sediments leaving the MD appears to go
1448 580 through cycles of trapping and resuspension in the estuary, before being partially advected
1449 581 seaward on the subaqueous delta and alongshelf, where they are largely incorporated into
1450 582 fluid mud along the bottom salinity front. The fluid muds have far-reaching effects on the
1451 583 coasts by reducing boundary shear stresses, attenuating of waves over a soft muddy bottom,
1452 584 affecting water-column /seabed exchanges, and serving as the agent of outward growth of the
1453 585 subaqueous delta (Marchesiello et al., 2019). In addition, fluid mud layers can lead to rise in
1454 586 fluid viscosity and density, and the reduction of bottom shear stresses can affect on the tidal
1455 587 wave propagation (Gabioux et al., 2005). Thus without flocculation, the particles would be
1456 588 carried directly offshore (Kineke et al., 1996). The appearance of fluid mud layer under
1457 589 flocculation regime provides a mechanism for rapid and strong sedimentation in the estuaries
1458 590 and lead to local siltation and mud accretion. Once deposited in the bed, fluid mud layers
1459 591 contribute to bedform development and stability (Schindler et al., 2015). We should underline
1460 592 that bedform consolidation and stability is hardly predictable, because it depends on both
1461 593 physical and biological near bed processes (Parson et al., 2016) that evolve continuously for
1462 594 sediment mixtures containing cohesive mud and biologically active substances such as
1463 595 microorganisms, bacteria and microphytobenthos who form biofilms (Malarkey et al., 2015).

1464 596 How can we anticipate the impact of human activities on sediment dynamics, flocculation and
1465 597 fluid mud layer formation at regional scale? As reported in the recent publications of Schmitt
1466 598 et al. (2017) and Thi Ha et al. (2018), human pressure, through sediment trapping and sand
1467 599 mining, already leads to a significant decrease of SSC in the estuaries. Our study points out
1468 600 that SSC is a determining factor affecting, first flocculation, and secondly, the formation of
1469 601 fluid mud layers in the Mekong estuary. There is a critical treshold of around $SSC = 0.4 \text{ g.L}^{-1}$,
1470 602 that can be seen as a tipping point for sediment processes. If the occurrence of SSC beyond
1471 603 that point decreases, the deposition rate will strongly reduce (no linear effects), while the
1472 604 erosion rate will probably increase because of a decrease of sediment quantity, and because of
1473 605 the reduction of drag coefficient in the regions of fluid muds (Dyer et al., 2002a), which
1474 606 enhances boundary shear stresses nearshore, coinciding with erosional areas in the Mekong
1475 607 estuaries (Kineke et al., 1996). As fluid mud layers in the Mekong estuaries are a key factor to

1499
1500
1501 608 promote flocculation and “boost” natural sedimentation, we do believe that some regular
1502
1503 609 monitoring programs should be realized. In terms of coastal management, a simple measure
1504
1505 610 that should be seriously considered is mangrove reforestation. Because of cohesiveness,
1506
1507 611 sediment particles transported out into mangrove forests during tidal inundation flocculate and
1508
1509 612 form larger flocs. Thus mangroves are not just passive colonisers of mud banks but they are
1510
1511 613 active in trapping suspended sediment, with positive feedback on shore protection (Furukawa
1512
1513 614 et al., 1997; Anthony and Gratiot, 2012; Gratiot and Anthony, 2016). This mechanism was
1514
1515 615 recently characterized through a deep geomorphological study conducted along the muddy
1516
1517 616 coast of the Guianas. In this environment, which is comparable to the Mekong shore, Brunier
1518
1519 617 et al. (2019) observed and quantified some exceptional rates of muddy shoreline retreat
1520
1521 618 following mangrove removal for field rice production. Apart from this mechanism, mangroves
1522
1523 619 play a role as a buffer between sea and land to prevent river sediment from re-entrainment to
1524
1525 620 the ocean at ebb tide (Furukawa and Wolanski, 1996).

1523 621 **5. Conclusions**

1524
1525 622 Field surveys and laboratory analysis were performed at regional scale in the upper fluvial,
1526
1527 623 lacustrine and lower estuarine environments to provide a physically-based assessment of
1528
1529 624 sediment transport regimes, flocculation, and fluid mud layer dynamics along the Lower
1530
1531 625 Mekong River (LMR). The independent evaluation of particle size and settling velocity
1532
1533 626 provides a good assessment of particles behaviour, and allows characterizing the R_0 number
1534
1535 627 and corresponding regimes in a robust way. Suspended sediments in fluvial and lacustrine
1536
1537 628 environments are predominantly flocculi (97 % and 100 % of total volume, respectively) and
1538
1539 629 primary particles, the modes are transported as washload or with a regime of strong
1540
1541 630 suspension. Some of these particles (primary particles and flocculi) probably experience
1542
1543 631 phases of deposition and resuspension, mostly in the adjacent floodplain, during their routing
1544
1545 632 through the Mekong basin, but we observed comparable sub distributions for fluvial,
1546
1547 633 lacustrine and even estuarine environments. This finding indicates that the primary particles
1548
1549 634 and flocculi populations very probably reach the estuary without any important physical
1550
1551 635 transformations (i.e. with similar PSD). In the estuary, the complex mixing between fluvial
1552
1553 636 and coastal waters and sediments offers optimal conditions of salinity, that leads to a higher
1554
1555 637 diversity of particles, with significant proportions of microflocs and macroflocs (25 % of total
1556
1557 638 volume), in the sand size range (diameter > 300 μm).

1558
1559
1560
1561
1562
1563
1564
1565
1566
1567
1568
1569
1570
1571
1572
1573
1574
1575
1576
1577
1578
1579
1580
1581
1582
1583
1584
1585
1586
1587
1588
1589
1590
1591
1592
1593
1594
1595
1596
1597
1598
1599
1600
1601
1602
1603
1604
1605
1606
1607
1608
1609
1610
1611
1612
1613
1614
1615
1616

639 The original estimation of flocculation indexes with SCAF instrument allows defining clearly
640 the flocculation regime. This later is the most efficient for SSC in the range of 0.4 – 4 g.L⁻¹. In
641 fluvial, lacustrine and estuarine environments, flocculation regime develops for the same
642 range of SSC, beyond ~0.4 g.L⁻¹. Flocculation then becomes a key process, but its impacts on
643 particles populations differs with the different environments. In the Tonle Sap lake,
644 flocculation promotes the aggregation of colloids and primary particles on flocculi. In the
645 estuarine environment, flocculation leads to the formation of a new population of particles, the
646 micro-flocs. In the fluvial environment, the data were too scarce to draw a clear conclusion, as
647 freshly eroded aggregates could not be yet in equilibrium with river hydro-sedimentary
648 conditions.

649 As a consequence of these microscopic changes at scales of particles, our study confirms the
650 regular occurrence of fluid mud layers (55 - 60% of occurrence) near bottom in the Mekong
651 delta with distance of less than 120 km from the coastline, concentrated in 30 km in both high
652 - and low - flow seasons. Fluid mud layers, which are intrinsically linked with flocculation
653 processes, are early steps of landforms evolutions and participate to the geomorphology of the
654 Mekong Delta (MD). In the light of this study and considering the degree of vulnerability of
655 the delta to ongoing hydro-sedimentary changes, we may provide two recommendations:
656 Firstly, the continental sediment flux needs to be restored (or at least maintained) and human
657 driven subsidence needs to be controlled. Under those conditions, fluid mud layers should
658 remain a driver of river and coastal geomorphology, as it has been the case over the last
659 millennia. Secondly, the perception of mangrove should be reconsidered as reforestation is
660 probably the optimal manner, in both technical and environmental aspects, for ensuring
661 sediment trapping and preserving fluid mud layers and mudflat, with positive feedbacks on
662 mangrove colonization. In other words, mangroves cannot compensate regional
663 disequilibrium in sediment balance, but they can facilitate the transformation of diluted
664 suspended sediment into fluid mud layers.

665 Taking into account the degree of uncertainty of field and laboratory measurements with
666 natural fresh sediments, and the degree of variability of sediment properties in such large and
667 human-impacted systems, there is a clear interest to adopt a monitoring strategy that would
668 extend the study in time and space.

669

1617
1618
1619
1620
1621
1622
1623
1624
1625
1626
1627
1628
1629
1630
1631
1632
1633
1634
1635
1636
1637
1638
1639
1640
1641
1642
1643
1644
1645
1646
1647
1648
1649
1650
1651
1652
1653
1654
1655
1656
1657
1658
1659
1660
1661
1662
1663
1664
1665
1666
1667
1668
1669
1670
1671
1672
1673
1674
1675

670 **Acknowledgements**

671 The authors would like to thank the Université catholique de Louvain, Belgium for Hoang-
672 Anh Le's doctoral fellowship, the Institut de Recherche pour le Développement (IRD -
673 France) to support the field surveys in Laos and in Vietnam with the financial support of
674 the Lower Mekong Delta coastal zones project (<http://lmdcz.siwrr.org.vn>). We also would like
675 to thanks VolTransMESKONG CNES/TOSCA project to support the monitoring in Cambodia
676 with the technical and scientific support of staff from LOG UMR8187 and the Institute of
677 Technology of Cambodia, especially.

678 **References**

679 1. Anthony, E. J., & Gratiot, N. (2012). Coastal engineering and large-scale mangrove
680 destruction in Guyana, South America: Averting an environmental catastrophe in the
681 making. *Ecological Engineering*, 47, 268-273.

682 2. Anthony, E.J., (2015). Wave influence in the construction, shaping and destruction of river
683 deltas: A review. *Marine Geology*, 361, 53-78.

684 3. Antoine, G., Cazilhac, M., Monnoyer, Q., Jodeau, M., Gratiot, N., Besnier, A. L., ... & Le
685 Brun, M. (2015, April). Lateral and vertical heterogeneity of flow and suspended sediment
686 characteristics during a dam flushing event, in high velocity conditions. In EGU General
687 Assembly Conference Abstracts (Vol. 17).

688 4. Azhikodan, G., & Yokoyama, K. (2018). Sediment transport and fluid mud layer formation
689 in the macro-tidal Chikugo river estuary during a fortnightly tidal cycle. *Estuarine, Coastal
690 and Shelf Science*, 202, 232-245.

691 5. Azrulhisham, E. A., & Azri, M. A. (2018, February). Application of LISST instrument for
692 suspended sediment and erosive wear prediction in run-of-river hydropower plants.
693 In 2018 IEEE International Conference on Industrial Technology (ICIT) (pp. 886-891).
694 IEEE.

695 6. Bachmann, R. W., Hoyer, M. V., Vinzon, S. B., & Daniel Jr, E. C. (2005). The origin of
696 the fluid mud layer in Lake Apopka, Florida. *Limnology and Oceanography*, 50(2), 629-
697 635.

698 7. Balica, S., Dinh, Q., Popescu, I., Vo, T. Q., & Pham, D. Q. (2014). Flood impact in the
699 Mekong delta, Vietnam. *Journal of Maps*, 10(2), 257-268.

1676
1677
1678
1679
1680
1681
1682
1683
1684
1685
1686
1687
1688
1689
1690
1691
1692
1693
1694
1695
1696
1697
1698
1699
1700
1701
1702
1703
1704
1705
1706
1707
1708
1709
1710
1711
1712
1713
1714
1715
1716
1717
1718
1719
1720
1721
1722
1723
1724
1725
1726
1727
1728
1729
1730
1731
1732
1733
1734

- 700 8. Brunier, G., Anthony, E. J., Gratiot, N., & Gardel, A. (2019). Exceptional rates and
701 mechanisms of muddy shoreline retreat following mangrove removal. *Earth Surface
702 Processes and Landforms*.
- 703 9. Camenen, B., & van Bang, D. P. (2011). Modelling the settling of suspended sediments for
704 concentrations close to the gelling concentration. *Continental Shelf Research*, 31(10),
705 S106-S116.
- 706 10. Camenen, B., Le Coz, J., Dramais, G., Peteuil, C., Fretaud, T., Falgon, A., ... & Moore, S.
707 A. (2014). A simple physically-based model for predicting sand transport dynamics in the
708 Lower Mekong River. In *Proc. River Flow conference*, Lausanne, Switzerland, 8p.
- 709 11. Castro-Orgaz, O., Giráldez, J. V., Mateos, L., & Dey, S. (2012). Is the von Kármán
710 constant affected by sediment suspension?. *Journal of Geophysical Research: Earth
711 Surface*, 117(F4).
- 712 12. Comba, S., & Sethi, R. (2009). Stabilization of highly concentrated suspensions of iron
713 nanoparticles using shear-thinning gels of xanthan gum. *Water Research*, 43(15), 3717-
714 3726.
- 715 13. Darby, S. E., Hackney, C. R., Leyland, J., Kumm, M., Lauri, H., Parsons, D. R., ... &
716 Aalto, R. (2016). Fluvial sediment supply to a mega-delta reduced by shifting tropical-
717 cyclone activity. *Nature*, 539(7628), 276.
- 718 14. Droppo, I. G., Nackaerts, K., Walling, D. E., & Williams, N. (2005). Can flocs and water
719 stable soil aggregates be differentiated within fluvial systems?. *Catena*, 60(1), 1-18.
- 720 15. Dyer, K. R., Bale, A. J., Christie, M. C., Feates, N., Jones, S., & Manning, A. J. (2002).
721 The turbidity maximum in a mesotidal estuary, the Tamar Estuary, UK: I. Dynamics of
722 suspended sediment. In *Proceedings in Marine Science* (Vol. 5, pp. 203-218). Elsevier.
- 723 16. Dyer, K. R., Bale, A. J., Christie, M. C., Feates, N., Jones, S., & Manning, A. J. (2002b).
724 The turbidity maximum in a mesotidal estuary, the Tamar estuary, UK: II. The flocculation
725 properties. In *Proceedings in Marine Science* (Vol. 5, pp. 219-232). Elsevier.
- 726 17. Edmonds, D. A., & Slingerland, R. L. (2010). Significant effect of sediment cohesion on
727 delta morphology. *Nature Geoscience*, 3(2), 105.
- 728 18. Eidam, E. F., Nittrover, C. A., Ogston, A. S., DeMaster, D. J., Liu, J. P., Nguyen, T. T., &
729 Nguyen, T. N. (2017). Dynamic controls on shallow clinoform geometry: Mekong Delta,
730 Vietnam. *Continental Shelf Research*, 147, 165-181.
- 731 19. Farrell, E. J., & Sherman, D. J. (2013). Estimates of the Schmidt Number for vertical flux
732 distributions of wind-blown sand. *Journal of Coastal Research*, 65(sp2), 1289-1295.

1735
1736
1737 733 20. Fennessy, M. J., Dyer, K. R., & Huntley, D. A. (1994). Size and settling velocity
1738 distributions of flocs in the Tamar Estuary during a tidal cycle. *Netherland Journal of*
1739 734 *Aquatic Ecology*, 28(3-4), 275-282.
1740 735
1742 736 21. Fettweis, M., Francken, F., Pison, V., & Van den Eynde, D. (2006). Suspended particulate
1743 matter dynamics and aggregate sizes in a high turbidity area. *Marine Geology*, 235(1-4),
1744 737 63-74.
1745 738
1747 739 22. Furukawa, K., & Wolanski, E. (1996). Sedimentation in mangrove forests. *Mangroves and*
1748 740 *Salt Marshes*, 1(1), 3-10.
1750 741 23. Furukawa, K., Wolanski, E., & Mueller, H. (1997). Currents and sediment transport in
1751 mangrove forests. *Estuarine, Coastal and Shelf Science*, 44(3), 301-310.
1752 742
1753 743 24. Gabioux, M., Vinzon, S. B., & Paiva, A. M. (2005). Tidal propagation over fluid mud
1754 layers on the Amazon shelf. *Continental Shelf Research*, 25(1), 113-125.
1755 744
1756 745 25. Gratiot, N., Gardel, A. and Anthony, E.J., 2007. Trade-wind waves and mud dynamics on
1757 the French Guiana coast, South America: input from ERA-40 wave data and field
1758 746 investigations. *Marine Geology*. 236, 15-26.
1759 747
1761 748 26. Gratiot, N., Coulaud, C., Legout, C., Mercier, B., Mora, H., & Wendling, V. (2015). Unit
1762 for measuring the falling speed of particles in suspension in a fluid and device comprising
1763 749 at least one measuring unit and one automatic sampler. Patent - Publication number
1764 750 WO2015055963 A, 1.
1765 751
1767 752 27. Gratiot, N., & Anthony, E. J. (2016). Role of flocculation and settling processes in
1768 development of the mangrove-colonized, Amazon-influenced mud-bank coast of South
1769 753 America. *Marine Geology*, 373, 1-10.
1770 754
1772 755 28. Gratiot, N., Bildstein, A., Anh, T. T., Thoss, H., Denis, H., Michallet, H., & Apel, H.
1773 (2017). Sediment flocculation in the Mekong River estuary, Vietnam, an important driver
1774 756 of geomorphological changes. *Comptes Rendus Geoscience*, 349(6-7), 260-268.
1775 757
1777 758 29. Gugliotta, M., Saito, Y., Nguyen, V. L., Ta, T. K. O., & Tamura, T. (2019). Sediment
1778 distribution and depositional processes along the fluvial to marine transition zone of the
1779 759 Mekong River delta, Vietnam. *Sedimentology*, 66(1), 146-164.
1780 760
1782 761 30. Gupta, A., & Liew, S. C. (2007). The Mekong from satellite imagery: A quick look at a
1783 762 large river. *Geomorphology*, 85(3-4), 259-274.
1784
1785 763 31. Hai, P. T., Masumoto, T., & Shimizu, K. (2008). Development of a two-dimensional finite
1786 element model for inundation processes in the Tonle Sap and its environs. *Hydrological*
1787 764 *Processes: An International Journal*, 22(9), 1329-1336.
1788 765
1789
1790
1791
1792
1793

1794
1795
1796
1797
1798
1799
1800
1801
1802
1803
1804
1805
1806
1807
1808
1809
1810
1811
1812
1813
1814
1815
1816
1817
1818
1819
1820
1821
1822
1823
1824
1825
1826
1827
1828
1829
1830
1831
1832
1833
1834
1835
1836
1837
1838
1839
1840
1841
1842
1843
1844
1845
1846
1847
1848
1849
1850
1851
1852

- 766 32. Hung, N. N., Delgado, J. M., Güntner, A., Merz, B., Bárdossy, A., & Apel, H. (2014).
767 Sedimentation in the floodplains of the Mekong Delta, Vietnam Part II: deposition and
768 erosion. *Hydrological Processes*, 28(7), 3145-3160.
- 769 33. Kineke, G. C., Sternberg, R. W., Trowbridge, J. H., & Geyer, W. R. (1996). Fluid-mud
770 processes on the Amazon continental shelf. *Continental Shelf Research*, 16(5-6), 667-696.
- 771 34. Kondolf, G. M., Rubin, Z. K., & Minear, J. T. (2014). Dams on the Mekong: Cumulative
772 sediment starvation. *Water Resources Research*, 50(6), 5158-5169.
- 773 35. Kummu, M., & Sarkkula, J. (2008). Impact of the Mekong River flow alteration on the
774 Tonle Sap flood pulse. *AMBIO: AMBIO*, 37(3), 185-193.
- 775 36. Kummu M, Tes S, Yin S, Adamson P, Jozsa J, Koponen J, Richey J, Sarkkula J (2014)
776 Water balance analysis for the Tonle Sap Lake - floodplain system. *Hydrological*
777 *Processes* 28(4):1722-1733.
- 778 37. Le, H. A., Lambrechts, J., Ortled, S., Gratiot, N., Deleersnijder, E., Soares-Fraza, S.,
779 (2019). An implicit wetting - drying algorithm for the Discontinuous Galerkin method:
780 Application to the Tonle Sap, Mekong River Basin. *Environmental Fluid Mechanics* (in
781 submission).
- 782 38. Lee, B. J., Fettweis, M., Toorman, E., & Molz, F. J. (2012). Multimodality of a particle
783 size distribution of cohesive suspended particulate matters in a coastal zone. *Journal of*
784 *Geophysical Research: Oceans*, 117(C3).
- 785 39. Malarkey, J., Baas, J. H., Hope, J. A., Aspden, R. J., Parsons, D. R., Peakall, J., ... & Bass,
786 S. J. (2015). The pervasive role of biological cohesion in bedform development. *Nature*
787 *communications*, 6, 6257.
- 788 40. Manh, N.V., Dung, N.V., Hung, N.N., Merz, B., & Apel, H. (2014). Large-scale
789 quantification of suspended sediment transport and deposition in the Mekong
790 Delta. *Hydrology and Earth System Sciences Discussions*, 11(4).
- 791 41. Manh, N.V, Dung, N. V., Hung, N. N., Kummu, M., Merz, B., & Apel, H. (2015). Future
792 sediment dynamics in the Mekong Delta floodplains: Impacts of hydropower
793 development, climate change and sea level rise. *Global and Planetary Change*, 127, 22-33.
- 794 42. Manning, A. J., Friend, P. L., Prowse, N., & Amos, C. L. (2007). Estuarine mud
795 flocculation properties determined using an annular mini-flume and the LabSFLOC
796 system. *Continental Shelf Research*, 27(8), 1080-1095.
- 797 43. Manning, A. J., Baugh, J. V., Spearman, J. R., & Whitehouse, R. J. (2010). Flocculation
798 settling characteristics of mud: sand mixtures. *Ocean dynamics*, 60(2), 237-253.

1853
1854
1855
1856
1857
1858
1859
1860
1861
1862
1863
1864
1865
1866
1867
1868
1869
1870
1871
1872
1873
1874
1875
1876
1877
1878
1879
1880
1881
1882
1883
1884
1885
1886
1887
1888
1889
1890
1891
1892
1893
1894
1895
1896
1897
1898
1899
1900
1901
1902
1903
1904
1905
1906
1907
1908
1909
1910
1911

- 799 44. Manning, A.J., Baugh, J.V., Soulsby, R.L., Spearman, J.R., Whitehouse, R.J.S., 2011a.
800 Cohesive sediment flocculation and the application to settling flux modelling (Chapter 5).
801 In: Ginsberg, Silvia Susana (Ed.), Sediment Transport. InTech, Vienna, ISBN: 978-953-
802 307-189-3, pp. 91–116.
- 803 45. Manning, A. J., Baugh, J. V., Spearman, J. R., Pidduck, E. L., & Whitehouse, R. J.
804 (2011b). The settling dynamics of flocculating mud-sand mixtures: Part 1—Empirical
805 algorithm development. *Ocean Dynamics*, 61(2-3), 311-350.
- 806 46. Marchesiello, P., Nguyen, N.M., Gratiot, N., Loisel, H., Anthony, E.J. and Nguyen, T.,
807 2019. Erosion of the coastal Mekong delta: Assessing natural against man induced
808 processes. *Continental Shelf Research*, 181, 72-89.
- 809 47. McAnally, W. H., Friedrichs, C., Hamilton, D., Hayter, E., Shrestha, P., Rodriguez, H., ...
810 & ASCE Task Committee on Management of Fluid Mud. (2007). Management of fluid
811 mud in estuaries, bays, and lakes. I: Present state of understanding on character and
812 behavior. *Journal of Hydraulic Engineering*, 133(1), 9-22.
- 813 48. McLachlan, R. L., Ogston, A. S., & Allison, M. A. (2017). Implications of tidally - varying
814 bed stress and intermittent estuarine stratification on fine-sediment dynamics through the
815 Mekong's tidal river to estuarine reach. *Continental Shelf Research*, 147, 27-37.
- 816 49. Mehta, A. J. (1991). Understanding fluid mud in a dynamic environment. *Geo-Marine*
817 *Letters*, 11(3-4), 113-118.
- 818 50. Mekong River Commission portal, available at <http://www.mrcmekong.org/>.
- 819 51. Mikkelsen, O. A., Hill, P. S., & Milligan, T. G. (2006). Single-grain, microfloc and
820 macrofloc volume variations observed with a LISST-100 and a digital floc
821 camera. *Journal of Sea Research*, 55(2), 87-102.
- 822 52. Milliman, J. D., & Meade, R. H. (1983). World-wide delivery of river sediment to the
823 oceans. *The Journal of Geology*, 91(1), 1-21.
- 824 53. Nguyen, T. T., Némery, J., Gratiot, N., Garnier, J., Strady, E., Tran, V. Q., ... & Aimé, J.
825 (2019). Phosphorus adsorption/desorption processes in the tropical Saigon River estuary
826 (Southern Vietnam) impacted by a megacity. *Estuarine, Coastal and Shelf Science*,
827 106321.
- 828 54. Nittrouer, C. A., DeMaster, D. J., Eidam, E. F., Nguyen, T. T., Liu, J. P., Ogston, A. S., &
829 Phung, P. V. (2017). The Mekong continental shelf: The primary sink for deltaic sediment
830 particles and their passengers. *Oceanography*, 30(3), 60-70.

1912
1913
1914
1915
1916
1917
1918
1919
1920
1921
1922
1923
1924
1925
1926
1927
1928
1929
1930
1931
1932
1933
1934
1935
1936
1937
1938
1939
1940
1941
1942
1943
1944
1945
1946
1947
1948
1949
1950
1951
1952
1953
1954
1955
1956
1957
1958
1959
1960
1961
1962
1963
1964
1965
1966
1967
1968
1969
1970

- 831 55. Nowacki, D. J., Ogston, A. S., Nittrouer, C. A., Fricke, A. T., & Van, P. D. T. (2015).
832 Sediment dynamics in the lower Mekong River: Transition from tidal river to
833 estuary. *Journal of Geophysical Research: Oceans*, 120(9), 6363-6383.
- 834 56. Parsons, D. R., Schindler, R. J., Hope, J. A., Malarkey, J., Baas, J. H., Peakall, J., ... &
835 Aspden, R. J. (2016). The role of biophysical cohesion on subaqueous bed form
836 size. *Geophysical research letters*, 43(4), 1566-1573.
- 837 57. Peteuil, C., Frétaud, T., Wirz, C., Camenen, B., Guertault, L., Le Coz, J., & Dramais, G.
838 (2014). Importance of field observation for managing sediment fluxes in hydropower
839 projects design and operation. In *Proceedings of the 19th IAHR-APD Congress, Hanoi,*
840 *Vietnam.*
- 841 58. Ribolzi, O., Evrard, O., Huon, S., Rouw, A. De, Silvera, N., Latschack, O., Soulileuth, B.,
842 Lefèvre, I., Pierret, A., 2017. From shifting cultivation to teak plantation: effect on
843 overland flow and sediment yield in a montane tropical catchment. *Sci. Rep.* 1–12.
- 844 59. Rijn, L. C. V. (1984). Sediment transport, part II: suspended load transport. *Journal of*
845 *Hydraulic Engineering*, 110(11), 1613-1641.
- 846 60. Rouse, H. (1937). Modern conceptions of the mechanics of fluid turbulence. *Trans*
847 *ASCE*, 102, 463-505.
- 848 61. Santini, W., Camenen, B., Coz, J. L., Vauchel, P., Guyot, J. L., Lavado, W., ... & Espinoza
849 Villar, R. (2019). An index concentration method for suspended load monitoring in large
850 rivers of the Amazonian foreland. *Earth Surface Dynamics*, 7(2), 515-536.
- 851 62. Schindler, R. J., Parsons, D. R., Ye, L., Hope, J. A., Baas, J. H., Peakall, J., ... & Paterson,
852 D. M. (2015). Sticky stuff: Redefining bedform prediction in modern and ancient
853 environments. *Geology*, 43(5), 399-402.
- 854 63. Schmitt, R. J. P., Rubin, Z., & Kondolf, G. M. (2017). Losing ground-scenarios of land
855 loss as consequence of shifting sediment budgets in the Mekong
856 Delta. *Geomorphology*, 294, 58-69.
- 857 64. Schelske, C. L. (2006). Comment on the origin of the “fluid mud layer” in Lake Apopka,
858 Florida. *Limnology and Oceanography*, 51(5), 2472-2480.
- 859 65. Seah, K. C., Qasim, G. H., Hong, Y. S., Kim, E., Kim, K. T., & Han, S. (2017).
860 Assessment of colloidal copper speciation in the Mekong River Delta using diffusive
861 gradients in thin film techniques. *Estuarine, Coastal and Shelf Science*, 188, 109-115.
- 862 66. Sequioa. LISST-Portable|XR User's Manual Version 1.2 (2016).
- 863 67. Siev S, Paringit EC, Yoshimura C, Hul S (2016) Seasonal Changes in the Inundation Area
864 and Water Volume of the Tonle Sap River and Its Floodplain. *Hydrology* 3(4):33-45.

1971
1972
1973
1974
1975
1976
1977
1978
1979
1980
1981
1982
1983
1984
1985
1986
1987
1988
1989
1990
1991
1992
1993
1994
1995
1996
1997
1998
1999
2000
2001
2002
2003
2004
2005
2006
2007
2008
2009
2010
2011
2012
2013
2014
2015
2016
2017
2018
2019
2020
2021
2022
2023
2024
2025
2026
2027
2028
2029

- 865 68. Sim, S. Y., Chan, D. C. H., Huang, T. F., Chai, W., Isaacson, T., Flood Jr, J. C., ... &
866 Orzen, M. (2007). U.S. Patent No. 7,272,613. Washington, DC: U.S. Patent and
867 Trademark Office.
- 868 69. Sime, L. C., Ferguson, R. I., & Church, M. (2007). Estimating shear stress from moving
869 boat acoustic Doppler velocity measurements in a large gravel bed river. *Water Resources*
870 *Research*, 43(3).
- 871 70. Smardon, R. (2009). Restoration of the Tram Chim National Wildlife Preserve, Vietnam.
872 *Sustaining the World's Wetlands*, 153–178.
- 873 71. Sottolichio, A., Hurther, D., Gratiot, N., Bretel, P., 2011. Acoustic turbulence
874 measurements of near-bed suspended sediment dynamics in highly turbid waters of a
875 macrotidal estuary. *Continental Shelf Research*, 31, S36-S49.
- 876 72. Spearman, J., & Manning, A. J. (2008). On the significance of mud transport algorithms
877 for the modelling of intertidal flats. In *Proceedings in Marine Science* (Vol. 9, pp. 411-
878 430). Elsevier.
- 879 73. Stokes, G. G. (1857). On the effect of wind on the intensity of sound. *Brit. Assoc.*
880 *Report*, 22.
- 881 74. Ta, T. K. O., Nguyen, V. L., Tateishi, M., Kobayashi, I., Tanabe, S., & Saito, Y. (2002).
882 Holocene delta evolution and sediment discharge of the Mekong River, southern
883 Vietnam. *Quaternary Science Reviews*, 21(16-17), 1807-1819.
- 884 75. Thi Ha, D., Ouillon, S., & Van Vinh, G. (2018). Water and suspended sediment budgets in
885 the lower Mekong from high-frequency measurements (2009–2016). *Water*, 10(7), 846.
- 886 76. Toorman, E.A., Anthony, E., Augustinus, P.G.E.F., Gardel, A., Gratiot, N., Homenauth,
887 O., Huybrechts, N., Monbaliu, J., Moseley, K., Naipal, S. 2018. Interaction of mangroves,
888 coastal hydrodynamics and morphodynamics along the coastal fringes of the Guianas.
889 *Coastal research library series*, Springer book, pp 429-473.
- 890 77. Tran, D. D., Van Halsema, G., Hellegers, P. J., Hoang, L. P., Tran, T. Q., Kumm, M., &
891 Ludwig, F. (2018). Assessing impacts of dike construction on the flood dynamics of the
892 Mekong Delta. *Hydrology and Earth System Sciences*, 22(3).
- 893 78. Tri, V. K. (2012). Hydrology and hydraulic infrastructure systems in the Mekong Delta,
894 Vietnam. In *The Mekong Delta System* (pp. 49-81). Springer, Dordrecht.
- 895 79. Udo, K., & Mano, A. (2011). Application of Rouse's Sediment Concentration Profile to
896 Aeolian Transport: Is the suspension system for sand transport in air the same as that in
897 water?. *Journal of Coastal Research*, 2079-2083.

2030
2031
2032
2033
2034
2035
2036
2037
2038
2039
2040
2041
2042
2043
2044
2045
2046
2047
2048
2049
2050
2051
2052
2053
2054
2055
2056
2057
2058
2059
2060
2061
2062
2063
2064
2065
2066
2067
2068
2069
2070
2071
2072
2073
2074
2075
2076
2077
2078
2079
2080
2081
2082
2083
2084
2085
2086
2087
2088

898 80. Uncles, R. J., Stephens, J. A., & Law, D. J. (2006). Turbidity maximum in the macrotidal,
899 highly turbid Humber Estuary, UK: Flocs, fluid mud, stationary suspensions and tidal
900 bores. *Estuarine, Coastal and Shelf Science*, 67(1-2), 30-52.

901 81. Van, L. A., & Van Bang, D. P. (2013). Hindered settling of sand–mud flocs mixtures:
902 From model formulation to numerical validation. *Advances in Water Resources*, 53, 1-11.

903 82. Van Leussen, 1994. Estuarine macroflocs and their role in fine-grained sediment
904 transport. Ph.D. thesis, University of Utrecht, The Netherlands.

905 83. Vanoni, V. A. (1946). Transportation of suspended sediment by water. *Trans. of*
906 *ASCE*, 111, 67-102.

907 84. W.C. Rouse. U.S. Patent and Trademark Office (1938).

908 85. Wendling, V., Gratiot, N., Legout, C., Droppo, I. G., Coulaud, C., & Mercier, B. (2015).
909 Using an optical settling column to assess suspension characteristics within the free,
910 flocculation, and hindered settling regimes. *Journal of Soils and Sediments*, 15(9), 1991-
911 2003.

912 86. Windt, C., Ebrahimian, A., & Traver, R. Flow Characterization of Stormwater Runoff in
913 Philadelphia. In *World Environmental and Water Resources Congress 2017* (pp. 365-371).

914 87. Winterwerp, J. C. (2002). On the flocculation and settling velocity of estuarine
915 mud. *Continental Shelf Research*, 22(9), 1339-1360.

916 88. Winterwerp, J. C. (2011). Fine sediment transport by tidal asymmetry in the high-
917 concentrated Ems River: indications for a regime shift in response to channel
918 deepening. *Ocean Dynamics*, 61(2-3), 203-215.

919 89. Wolanski, E., Huan, N. N., Nhan, N. H., & Thuy, N. N. (1996). Fine-sediment dynamics in
920 the Mekong River estuary, Vietnam. *Estuarine, Coastal and Shelf Science*, 43(5), 565-582.

921 90. Wolanski, E., Nhan, N. H., & Spagnol, S. (1998). Sediment dynamics during low flow
922 conditions in the Mekong River estuary, Vietnam. *Journal of Coastal Research*, 472-482.

923 91. Xing, F., Meselhe, E. A., Allison, M. A., & Weathers III, H. D. (2017). Analysis and
924 numerical modeling of the flow and sand dynamics in the lower Song Hau channel,
925 Mekong Delta. *Continental Shelf Research*, 147, 62-77.

2089
2090
2091
2092
2093
2094
2095
2096
2097
2098
2099
2100
2101
2102
2103
2104
2105
2106
2107
2108
2109
2110
2111
2112
2113
2114
2115
2116
2117
2118
2119
2120
2121
2122
2123
2124
2125
2126
2127
2128
2129
2130
2131
2132
2133
2134
2135
2136
2137
2138
2139
2140
2141
2142
2143
2144
2145
2146
2147

926

Appendix

927 Fig. a, b, c display the detailed PSD for some representative samples collected in fluvial,
 928 lacustrine and estuarine environments, respectively. For clarity purposes, only a limited (nine)
 929 number of samples are represented in the first panel row. The second row exhibits
 930 representative PSDs without sonication and the last row is for representative PSDs with
 931 sonication. After two minutes of sonication, all three environments show higher percentages
 932 of smallest constituents, namely primary particles. The mean size of samples taken in the
 933 fluvial and lacustrine parts is smaller than ones taken in the estuary, especially after
 934 sonication, a considerable constituent of primary particles is found in the upper parts. In
 935 addition, the particle size in Tonle Sap was smallest, with mean diameter of approximately 7
 936 μm and primary particles are predominance. In contrast, the graphs illustrate the large
 937 variation of particle sizes in the delta, predominantly in range of 10 - 386 μm before
 938 sonication and 2.21 - 331 μm after sonication. It is clear that sand appears in the Mekong
 939 estuary with percentage of 11 %; a median diameter of $> 300 \mu\text{m}$.

(a) Fluvial

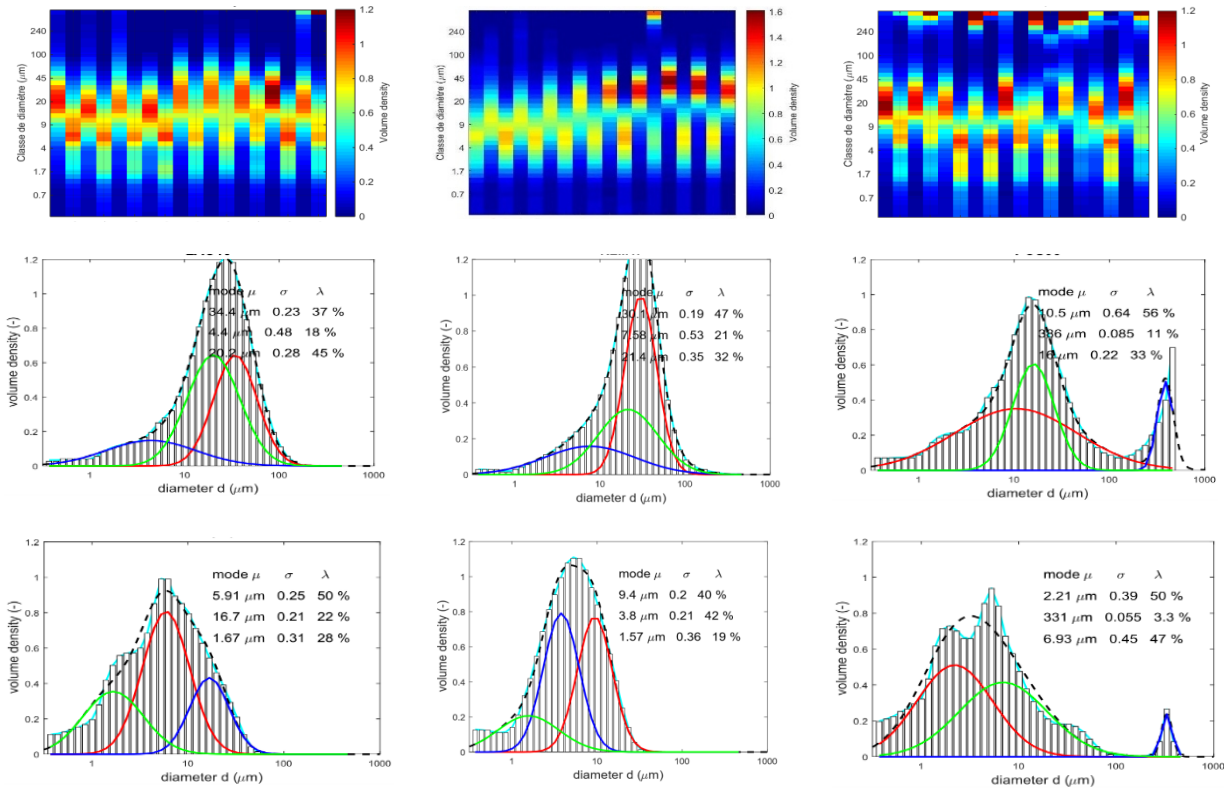
(b) Lacustrine

(c) Estuarine

Mekong river, Laos, 06/2017

Tonle Sap, Cambodia,
09/2018

Mekong estuary, Vietnam,
03/2016



940 Fig. PSD of three representative samples in fluvial, lacustrine and estuarine environments

Conflict of interests :

On behalf of co-authors, I declare no conflict of interests.